CHARACTERIZATION ANALYSIS OF SPATIAL LIGHT MODULATORS USING INTERFEROMETRY AND POLARIZATION

by

Cruz Yuliana Calderón Hermosillo

Thesis

Submitted to the Centro de Investigaciones

en Óptica A. C. for the degree of

Doctor in Sciences

Optics

June 2014

List of used acronyms

CIO	Centro de investigaciones en Óptica
CONACyT	Consejo nacional de ciencia y tecnología
EASLM	Electrically addressed SLM
FLCoS	Ferroelectric liquid crystals
ITO	Indium-Tin oxide
LC	Liquid crystal
LCoS	Liquid crystal on silicon
LC-SLM	Liquid crystal - spatial light modulator
OASLM	Optically addressed SLM
PWM	Pulse width modulation
RMS	Root mean square
SLM	Spatial light modulator
SOP	State of polarization
TN-LCD	Twisted nematic - liquid crystal display

Acknowledgments

To the glory of my God and Saviour, Jesus Christ. For from Him and Through Him and to Him are all things.

I want to thank my supervisor Jorge Luis García his support in this work. I also thank the financial support of CONACyT, the Mexican Council of Science and Technology (Scholarship Number 132073). Without its support, my studies would not have been made real.

I am grateful to my family. They are an example of great values in humankind: respect, generosity, patience, persistence and encouragement. These virtues make them an excellent guide. Their support has been instrumental to the happy conclusion of this path of personal growth.

Finally, I would also like to thank to the members of CIO, in particular Moisés Cywiak, Enrique Landgrave, Alexander Kiryanov, Daniel Malacara, Alejandro Téllez, David Moreno, Carlos Pérez, Daniel Donato and Manuel de la Torre for their helpful advice, ideas and comments. They are great examples of the empathy value in the lives of human beings.

Agradecimientos

A mi Dios y Salvador, Jesucristo. Porque de Él, y por Él, y para Él, son todas las cosas. A Él sea la gloria y la honra.

[1]Para mi asesor Jorge Luis García por su apoyo en este trabajo. Para el Consejo Nacional de Ciencia y Tecnología de México (Beca número 132073), sin cuyo respaldo mis estudios no hubieran sido posibles.

Para mi familia, muestra de grandes valores del ser humano: respeto, generosidad, persistencia, ánimo y paciencia; que los convierten en inmejorables guías. Su apoyo ha sido determinante para concluir venturosamente este camino de crecimiento personal.

Para los miembros del Centro de Investigaciones en Óptica que me apoyaron en numerosas ocasiones, en especial por sus valiosos comentarios, ideas y consejos. Son un gran ejemplo del valor de la empatía en la vida de los seres humanos.

[1] Spanish version of the Acknowledgments

Summary

This thesis deals with a method for the characterization of a spatial light modulator SLM using interferometry and polarization. A liquid crystal SLM display can alter the phase and amplitude of an incoming laser beam. It can be used to shape an incident beam into almost any arbitrary exit beam. However, an LCoS-SLM presents some negative effects: temporal fluctuations in phase and amplitude. These fluctuations are known as flicker. The first part of this thesis introduces the basic concepts for an SLM and presents a review of some methods to characterize an SLM.

This work shows experimental results of the proposed method with a Twyman-Green interferometer that uses polarized incident light and a commercial reflective LCoS-SLM. Furthermore, a computer model to analyze the accuracy of the proposed method was realized. Finally, the behavior of the flicker in an LCoS-SLM for different polarization schemes and temperatures is observed.

Contents

List of used acronyms II

Acknowledgments III

Agradecimientos IV

Summary V

Chapter 1. Introduction 1

Chapter 2. General description of an SLM device 4

2.1. Motivation 4

2.2. Types of SLMs 5

2.2.1. Optically Addressed SLM (OASLM) 5

2.2.2. Electrically Addressed SLM (EASLM) 7

2.3. SLM Technologies 8

2.4. SLM Operation Principle 9

Chapter 3. Methods to characterize SLMs 15

3.1. Measuring the Jones Matrix 16

3.2. Examining the polarization eigenvectors 17
3.3. By using Mueller-Stokes 18
3.4. By evaluating Fresnel images 20
3.5. By using lateral shearing interferometry 21
3.6. Using an interferometer 22
3.7. Flicker 24

Chapter 4. Phase shift assessment 25

4.1. Analysis 26
4.1.1. Interference 26
4.1.2. Moiré fringe patterns 28
4.1.3. Phase shift measurement method 31

Chapter 5. Characterizing the SLM 35

5.1. Experimental fringe patterns 37
5.1.1. The use of a single polarizer 40
5.1.2. The use of a polarizer-analyzer couple 42
5.2. Optimization 46
5.2.1. Moiré technique 46

Chapter 6. Flicker behavior in a TN LCoS-SLM 51

6.1. Flicker assessment 52
6.1.1. Flicker measurement method 52
6.1.2. Cooling process 53
6.2. Measurement in a polarization scheme 55
6.2.1. Scheme of linear vertical polarization 56
6.2.2. Scheme that minimizes flicker modulation 58
6.2.3. Scheme that maximizes phase modulation 60

Chapter 7. Conclusions 63

Bibliography 65

Chapter 1

Introduction

Considerable interest has been shown in the devices capable of converting electronic data into spatially modulated coherent optical signals. Such a device is called a *spatial light modulator* SLM [1].

An SLM is an electrically programmable device that modulates light according to a fixed spatial (pixel) pattern. SLMs have an expanding role in several optical areas where light control on a pixel-by-pixel basis is critical for optimum system performance. SLMs are typically used to control incident light in amplitude-only, phase-only or the combination of both [2].

The control of these amplitude and phase variations are useful in different photonics applications such as: Beam steering, optical tweezers, diffractive optics, optical correlation, optical waveform shaping, wavefront correction [3], ultra-fast pulse shaping, optical data processing, holographic data storage, programmable phase masks, image processing/analysis, etc. [4, 5, 6, 7].

Especially in vortex dynamics research, the fact that vortex parameters can be changed with the click of a button has made the SLM a popular

device. However, there are several disadvantages. The liquid crystal display is not made for high powers of incident light. Therefore, there is a maximum possible power in a beam modulated by an SLM.

LC-SLMs are polarization-sensitive devices, i.e., they primarily modulate the state of polarization SOP of an input beam. This change in the SOP to complex modulation had been studied by sandwiching the SLM between polarization elements, as linear polarizers and retarder plates [8, 9].

This thesis will deal mainly with the characterization of the complex modulation of an SLM. In order to reach this goal, an interferometric method using different polarization states of the incident beam is proposed; this method is optimized using moiré techniques. In this work two main contributions are presented. First, the maximum phase modulation with minimum amplitude modulation is achieved using only linearly polarized incident light without using an analyzer, and the amplitude modulation can be increased using the analyzer also. And second, the behavior of the flicker in an LCoS-SLM for different schemes of polarized light and temperatures is observed. This work shows experimental results with a Twyman-Green interferometer that uses a commercial reflective LCoS-SLM and is illuminated with polarized impinging light.

Chapter Two starts with the description of the two classes in which are categorized the SLMs, the description of the properties of liquid crystals, and then gives the main SLM technologies based on liquid crystals used in optical processing. Finally, the working principle behind an SLM is provided.

In Chapter Three, a review of the most common SLM characterization

methods that can be performed to ensure the correct working of the device, and some of the advantages that they offer are presented.

Chapter Four gives a relatively simple computer model that simulates the complex amplitude that can allow the use of a reflective spatial light modulator in a arm of a Twyman-Green interferometer under ideal conditions for phase shift assessment. This model gives an idea of the expected behavior of an SLM using an interferometric setup. This analysis is complemented with the extraction of the phase of moiré fringe patterns.

In Chapter Five, the experimental method explored to characterize the complex amplitude of an SLM is presented and evaluated.

Chapter Six deals with the problem of temporal fluctuations in phase and amplitude, also known as *flicker*, that is present in a twisted nematic SLM. The performance of the spatial light modulator under temperature modification and different polarization schemes is presented.

Finally, in Chapter Seven the conclusions are given.

Chapter 2

General description of an SLM device

A Spatial Light Modulator, abbreviated by SLM, is a device that spatially modulates a beam of coherent (or incoherent) light. This chapter begins with the types of SLMs, then describes the properties of liquid crystals and gives the most important technologies based on liquid crystals due to their applications in optical processing. Finally, it gives a description of the operation of an SLM.

2.1. Motivation

The manipulation of the shape of laser beams has been made easier and more flexible with the invention of the SLM. The most used SLMs work because of a liquid crystal display that is able to modulate the phase or amplitude of incident light. The display works in somewhat the same way as a regular LCD screen. The SLM display also has pixels that get their information either electrically or optically.

SLMs are used not only to input data to be processed, but also to create

spatial filters that can be modified in real time. In such a case the SLM is placed in the back focal plane of a Fourier transforming lens, where it modifies the transmitted amplitude of the fields in accord with a desired complex spatial filter [1].

2.2. Types of SLMs

There is a extensive categorization of SLMs into two classes that can be made: **Optically Addressed SLM (OASLM),** that converts incoherent light to spatial modulation, and **Electrically Addressed SLM (EASLM),** that converts electrical signals to spatial modulation.

Often a given SLM technology may have two different forms, one suitable for electrical addressing and one suitable for optical addressing [1].

2.2.1. Optically Addressed SLM (OASLM)

OASLMs can record, replay and erase images with a time-frame of a millisecond. During that time—frame an image is projected onto the photosensitive side of the OASLM using coherent or incoherent light. This image (write light) is absorbed within the photosensor and creates spatially varying charges. The charges move towards the two Indium-Tin Oxide (ITO) electrodes, with the aid of an electric field applied across the whole of the OASLM. This movement creates a spatially varying electric field, which modifies the state of the liquid crystals (modulating layer) and creates a replica of the projected image within the liquid crystal (LC) layer. The image can be read out from the LC layer using a second beam (read beam).

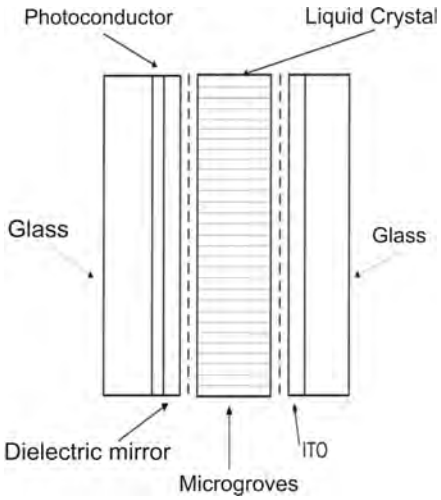

Figure 2.2.1. Basic structure of OASLM. Image adapted from [11].

The image can then be erased by applying an appropriate erase pulse on the device and in some cases applying a third beam (erase beam) [10].

In this case, the information may be input to the SLM in the form of an optical image at the start, rather than in electrical form [1].

The basic structure of a OASLM device is with the LC in a thin cell with surface groves [11] that align the molecules. Figure 2.2.1 shows the basic structure of the OASLM.

Optically addressed SLMs have several key properties besides their fast temporal response that are very useful for optical processing systems. First, they can convert incoherent images into coherent images, as alluded to above. Second, they can provide image amplification: a weak incoherent image input to an optically addressed SLM can be read out with an intense coherent source. Third, they can provide wavelength conversion: e.g. an incoherent image in the infrared could be used to control the amplitude transmittance of a device in the visible [1].

2.2.2. Electrically Addressed SLM (EASLM)

As its name suggest, the image on an electrically addressed spatial light modulator is created and changed electronically, as in most electronic displays. EASLMs usually receive input via a conventional interface such as VGA or DVI input. Electrical signals representing the information to be input to the system (perhaps in raster format) directly drive a device in such a way as to control its spatial distribution of absorption or phase shift [1]. Far more used than OASLM, also much more developed since they are useful outside field of coherent optical processing.[1]

An example of an EASLM is the digital micromirror device at the heart of LCoS displays using ferroelectric liquid crystals (FLCoS) or nematic liquid crystals.

[1] all ESLMs are pixelated. Leads to some diffraction problems when used in coherent optical systems [11].

2.3. SLM Technologies

Of the great number of different SLM technologies that have been studied, the liquid crystal devices have survived the longest and remain important devices in practice. There are many variants of these devices, some using nematic liquid crystals, and others using ferroelectric liquid crystals [1]. Furthermore, the ferroelectric SLMs are only able to modulate the phase in a binary manner (for example either 0 or π). Nematic SLMs can modulate the phase by a discrete range of values between 0 and 2π of phase stroke.

For a book on this subject covering the properties of more types of SLMs, including that of the liquid crystal on silicon LCoS used in this work, one can consult Ref. [1] and its associated references. It presents the properties of liquid crystals such as: mechanical properties, electrical properties and optical properties of liquid crystals.

Liquid Crystal over Silicon

Liquid crystal on silicon (LCoS) is a micro-display technology developed initially for projection televisions but now used also in Wavelength Selective Switches. It is a reflective technology similar to LC panels, but operate in reflection with control voltages supplied by mirrors on a silicon chip. Figure 2.3.1 shows the schematic design of a LCoS-SLM. The silicon backplane is then essentially a memory chip with reflective mirrors, it uses a liquid crystal layer on top of a silicon backplane instead of individual mirrors. By way of comparison, some LCD projectors use transmissive LCD, allowing light to pass through the liquid crystal.

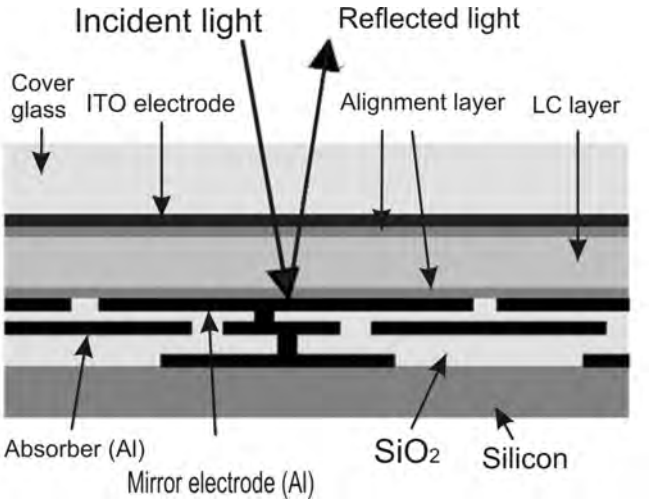

Figure 2.3.1. Schematic design of a LCoS-SLM. Image adapted from [12].

2.4. SLM Operation Principle

When choosing a liquid crystal SLM, there is the option of a ferroelectric or nematic device, depends on the application to be used. As mentioned in section 2.3, nematic SLM can modulate by a discrete range of values between 0 and 2π of phase stroke and a ferroelectric device in binary form.

The SLM used in this work is an electrically-addressed nematic liquid crystal one, figure 2.4.1 shows: a) Driver Output Panel, b) Driver Input Panel and c) Connected LCoS display.

This section describes the SLM operation principle focusing on liquid crystal on silicon (LCoS) technology. The technical parameters of the SLM used are:

Technical parameters

Display:

Type:	LCoS XGA Active Matrix LCD
Mode :	reflective, normal black TN
Display Grey Shades:	256 (8-bit) Grey Levels
Image Array Dimension:	19,5 x 14,6 mm^2
Resolution:	Nominal: 1024 H x 768 V
	Total: 1032 H x 776 V
Pixel Pitch:	19 µm
Fill Factor:	>93%
Image Frame Rate:	75 Hz
Contrast Ratio:	1000 :1
Response Time:	typ. 16 ms

Device:

Dimensions L x W x D:		165 x 44 x 120 mm^3
Weight:		ca. 0,75 kg
Power Supply:		
Prim.:	Voltage rating :	100-230 V
	Frequency:	50-60 Hz
	Power Input:	max. 12 VA
Sek.:	Voltage rating:	12 V DC
	Current rating:	max. 500 mA
Operating Conditions:		
	Operating Temperature:	+10° C to +30°C
	Operating Humidity:	30% to 75%

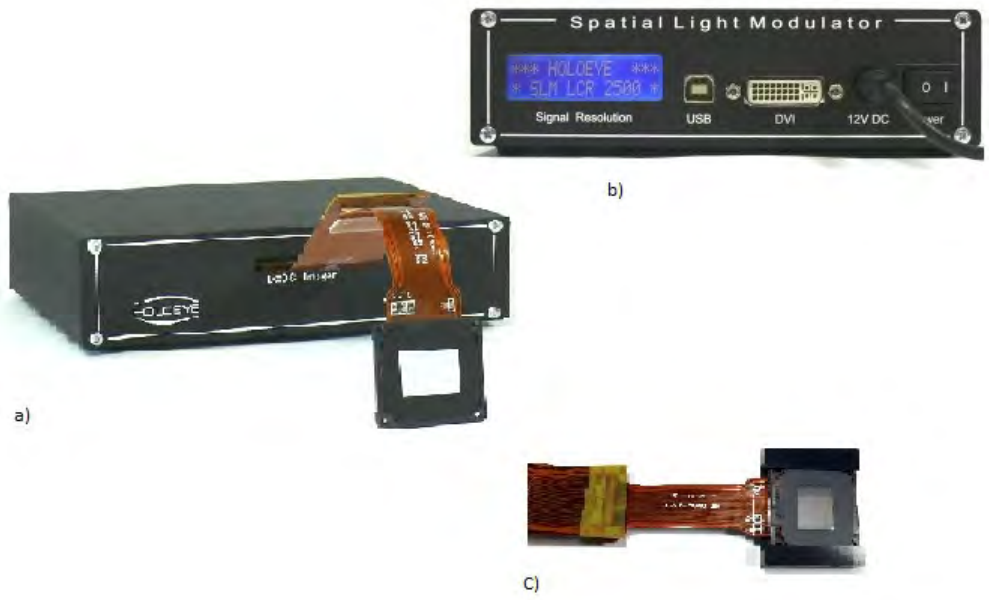

Figure 2.4.1. a) Driver Output Panel, b) Driver Input Panel and c) Connected LCoS display. Image adapted from [13].

The display of this SLM consists of birefringent liquid crystals. At the backside of the display are silicon pixelated electrodes and on the other side is a transparent electrode. Figure 2.4.2 shows the structure of the display of a reflective LCoS-SLM.

The reflective arrangement due to silicon backplane allows putting a high number of pixels in a small panel, keeping the fill factor ratio high even for micrometer-sized pixels.

In order to get a good reflectivity out of these reflective pixelated arrays, high reflective aluminum mirrors, most with a passivation layer, are used. Various techniques for planarization or reduced interpixel gap effects have been developed over the years [14].

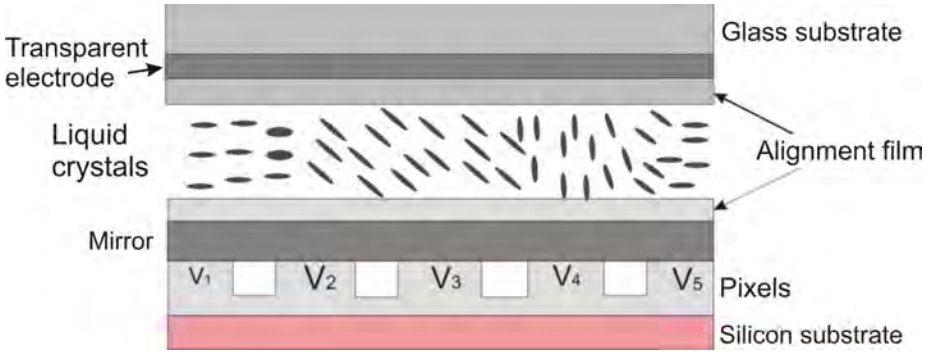

Figure 2.4.2. Each pixel has a different voltage applied. The liquid crystals orient themselves according to the applied voltage. The light protruding through the glass substrate receives half the user-set phase modulation due to the liquid crystal layer. The light is then reflected by the mirror, receives the other half of the phase modulation and exits the device through the glass substrate again. Image adapted from [16].

It is also possible to cover the backplane with a dielectric mirror so that the pixelated structure is not seen any more. It allows to increase the reflectivity of the SLM, so the light utilization efficiency for a low-frequency content is higher. Unfortunately, dielectric layers limit the spectral range of the device.

The orientation of the liquid crystals depends on the applied electric field. The molecules inside this liquid crystal have a cigar-like shape. If there is no electric field present, the cigars align themselves in a preferred direction due to the alignment films, see Figure 2.4.3.

Analog and digital drive schemes are used, and the differentiation is based on the actual generated voltage applied to individual pixels.

In a digital drive scheme a pulse width modulation (PWM) encodes a certain gray level into a series of binary pulses in the kilohertz range, referred to as a sequence. In principle, every individual pulse interacts with the LC

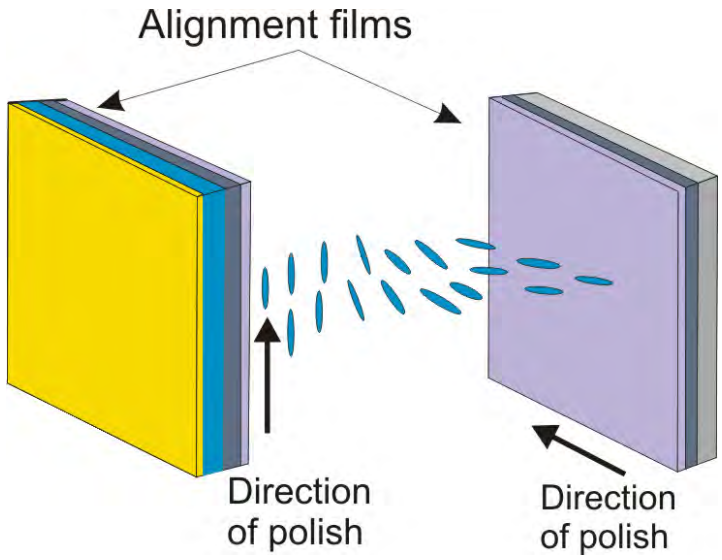

Figure 2.4.3. Molecular arrangements in a twisted nematic liquid crystal (no voltage applied).

molecule, causing its rotation, that at the end leads to the desired gray level representation. Owing to a limited rotational viscosity of the LC material, LC molecules cannot follow individual pulses of the electrical signal in a discrete way.

All pixels are addressed simultaneously, this represents a disadvantage, one observes a kind of flicker noise at high frequencies ("supermodulation"). This means the electro-optical response of the SLM is not constant over the frame [15].

When an increasing electric field is applied, the molecules begin to align themselves along the electric field (see Figure 2.4.4). This realignment causes the index of refraction of the crystal to change. The optical path length of the light (and therefore its phase) is altered when the refractive index changes. The effect is polarization dependent as the long axis of the liquid crystal

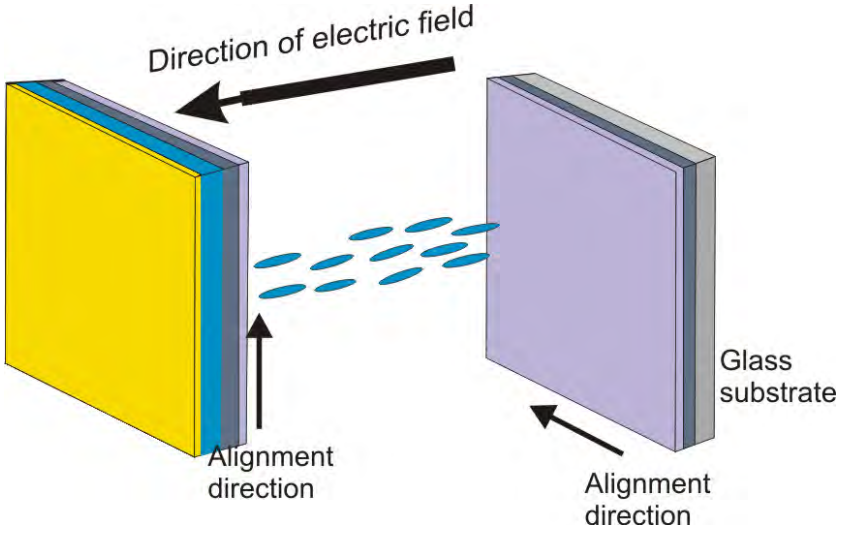

Figure 2.4.4. Twisted nematic liquid crystal with a voltage applied. Only a small column of molecules is shown.

causes the change. So, depending on the polarization state of the impinging light such refractive index variation may introduce phase and amplitude variations [16]. In this manner, a spatial light modulator allows control over the complex modulation applied to an incident beam.

Furthermore, the SLM only works for one polarization and monochromatic light (a technique for more broadband light sources was first demonstrated by Leach et al. [17]).

Chapter 3

Methods to characterize SLMs

By characterization we understand the measurement of the relevant parameters of the SLM such as: the amplitude modulation, the phase shifting ability, the flicker, the contrast, the surface flatness and the frame rate [12].

Nevertheless, every model proposed is limited to characterization of one or more parameters, and focused to optimize a specific application. Some of the models have to be verified either by other techniques resulting a time consuming sequential process. For example, the optimized complex modulation curve measured with the Jones matrix has to be verified either by interferometric techniques, such as the Mach-Zender and the Young double-slit interferometer, or by diffraction-based methods.

In this chapter, a brief revision of proposed methods to characterize SLMs is presented. The techniques reviewed here are limited to characterization of one or more parameters.

3.1. Measuring the Jones Matrix

Methods for the determination of the Jones matrix of liquid crystal displays (LCDs) employing a physical model of the modulator have been reported [18, 19, 20, 21, 22].

A model-free approach for measuring all eight parameters (including the signs) of the Jones matrices of liquid-crystal displays was presented by Kholer, Haist and Osten [23]. Such approach offers several advantages. No knowledge about the internal structure of the modulator is needed, it is applicable for perpendicular or oblique incident light, and it should be possible to characterize whole optical systems (e.g., including beam splitters or mirrors that influence the polarization). In most ellipsometric measurement methods, the Jones vectors are determined up to the sign of the phase difference between the two components of the Jones vector, which is not sufficient for the correct determination of a Jones matrix of an LCD. Another issue is that an interferometric reference is needed if the phase change between two switching states of the LCD must be determined. The method could be applied to measure the Jones matrices for all addressable gray levels thus delivering the specifications needed for calculating characteristic curves for arbitrary input and output polarizations. Unlike other approaches, they did not rely on a physical model of the LCD. Thus, it could be possible to measure the Jones matrices of a more complex optical system in one step (e.g., when a reflective LCD is used in combination with a beam splitter). Though the method presented is, in principle, applicable for transmissive and reflective LCDs, calculations and experiments were only shown using the example of a

reflective liquid-crystal-on-silicon display, LCoS-SLM. They focused on the use of an LCD with the aim of complex modulation of the incident light. For other applications, such as digital holography [24, 25], optical tweezers [26], or optical image processing, a phase-only or mixed-mode modulation is preferred. For detailed simulations of systems that employ LCDs, the complete Jones matrix of an LCD was needed [27]. The measurement of Jones matrices [28, 29, 30] as well as the characterization of LCDs by their amplitude and phase modulation (complex transmission) was a topic widely treated throughout literature [25, 31].

3.2. Examining the polarization eigenvectors

Pezzanitti and Chipman [18] introduced the concept of average polarization eigenstates. They experimentally determined the average polarization eigenvectors for an LCD.

Davis, I. Moreno and P. Tsai [19], derived theoretical expressions for these polarization eigenvectors using the Jones matrix introduced by Lu and Saleh [32]. Moreno, et al., presented an experimental verification of these Jones eigenvectors in twisted nematic liquid crystal displays [33].

Moreno et al. [34], proposed a method to phase-mostly modulation for a twisted nematic liquid crystal display (LCD) examining the polarization eigenvectors (using the Jones matrix formulation). They compared the reflective and transmissive properties (intensity transmission and phase shift) for an LCD. Their goal was phase-mostly modulation with a phase shift that exceeds 2π rad and the reflective geometry was of interest because the

phase modulation depth increases with the double pass. They examined the polarization eigenvectors for two reflective geometries, by including or not including a wave plate between the LCD and the mirror. The LCD behavior was modeled with a simplified physical model that uses two birefringence parameters that depend on the addressed gray level. They considered a geometry in which the transmissive eigenvector was sent through the LCD, reflected, and sent back again. They find that the experimental setup must be modified by adding a quarter-wave plate between the LCD and the mirror so that the reflected beam can be converted back into the appropriate eigenvector.

3.3. By using Mueller-Stokes

The polarimetric properties of a liquid crystal on silicon display (LCoS), including depolarization and diattenuation, normally were not considered when applying the LCoS in diffractive or adaptive optics. Characterization of a device showing depolarization to be used in amplitude-only or in phase-only modulation regimes, is a necessary study. In principle, it can be expected that depolarized light may be added incoherently as a non-uniform background across the aperture of the LCoS because the degree of polarization may depend on factors such as the addressed gray level and the incident state of polarization [35].

Wolfe and Chipman [36] showed that a full polarimetric characterization of LCoS devices is a more complete and suitable approach than the standard radiometric characterization typically followed by the display industry in

quality control tests [37]. In their study, they found a certain degree of depolarized light and the inhomogeneity in various polarimetric parameters across the LCoS aperture. The existence of depolarized light [38] may lead to the degradation in the application of the LCoS as an SLM. This effect cannot be calibrated and evaluated using the models described in Refs. [32, 39, 40, 41, 42].

The Mueller matrix formalism provides an alternative polarimetric description of polarization phenomena, and it has been also applied to calibrate the response of LCDs. Pezzanitti and Chipman [18] measured the Mueller matrix of an LCD to calculate its average eigenpolarization states in order to obtain phase-only modulation.

The Mueller matrix characterization enables for a numerical search of optimum intensity modulation configurations.

In this polarimetric study they included time measurements that show that the main phenomenon responsible for the depolarization is the temporal fluctuations, called *flicker*, of the state of polarization of the light reflected by the LCoS.

Márquez et al. [35], characterized the polarimetric properties of an LCoS, therefore including depolarization and diattenuation which are usually not considered when applying the LCoS in non-display applications. Along with the polarimetric characterization they measured the Mueller matrix of the LCoS as a function of the gray level and found that the LCoS generates a certain degree of depolarized light. They use the Stokes vector measurements to calculate the Mueller matrix for the LCoS.

They obtained the best results when used elliptically polarized light but

by means of a heuristic approach they showed that amplitude-mostly modulation or phase-mostly modulation with a large phase-shift modulation depth can be also obtained at a wavelength of 633 nm.

3.4. By evaluating Fresnel images

A lack of spatial uniformity in the phase response of a SLM can appear due to addressing errors or to factors that are voltage independent, for example, the curvature of the surface device, which causes variations in the LC thickness . In the case of the widely used liquid crystal on silicon (LCoS) displays, the reflected wavefronts can be distorted by the curvature of the silicon backplane . Typical magnitudes of these kinds of phase errors are of the order of λ over the aperture of the device.

It was shown by Guigay [43] and later found independently [44, 45, 46] that the Fresnel images of binary phase gratings, at multiples of certain fractions of the Talbot distance, exhibit binary intensity distributions, whose visibility depends on the phase step height. This property of Fresnel images has found numerous applications in various areas of physics [46, 47, 48, 49]. In the context of SLM calibration, the phase response of a twisted nematic LCD has been measured by displaying binary phase gratings of constant phase step height [45].

Martínez-León et. al. reported a method for calibrating SLMs based on the evaluation of Fresnel images [50]. The Fresnel images generated by a binary phase diffraction grating consists of binary irradiance distributions whose visibility depends on the phase modulation. They proposed a mod-

ification of [45], they displayed on their SLM a diffraction grating with a binary phase step along one direction and a linearly increasing phase along the orthogonal direction, performing a complete phase calibration. Thanks to this change, it is possible to observe the resulting distribution of the visibility function with a kind of carrier frequency fringe, and not in the uniform field to detect and measure the local addressing errors. In this way, the phase modulation for every pixel and for every value of the entrance signal could be determined experimentally. In this way, it is possible to check the degree of spatial uniformity of the SLM phase response with a very simple experimental set-up.

3.5. By using lateral shearing interferometry

The calibration of an TN-LCD for a given wavelength is a two-step procedure: (1) a polarimetric characterization is done by fitting the measured intensity transmission, for specific polarizations, to an assumed Jones [22] or Mueller matrix [51]; (2) the polarimetric matrix is then used to predict the modulation for arbitrary polarizations and numerical optimization techniques are employed to achieve a desired modulation curve [52].

The optimized complex modulation curve has to be verified either by interferometric techniques, such as the Mach-Zender [32] and the Young double-slit interferometer [53], or by diffraction-based methods [54]. While the diffractive techniques measure simultaneously the amplitude and phase modulation, most interferometric techniques are best suited for phase measurements, being the amplitude modulation measured separately with a

photometer. Nevertheless, all commonly used techniques measure a single modulation level at a time. A complete measure of a modulation curve thus requires a series of time consuming sequential measurements.

An interferometric technique based on an a shear plate was proposed [55] to measure phase modulation. Flávio P. Ferreira and Michael S. Belsley extended such technique to measure the complex modulation curve of a spatial light modulator [56]. Based on a lateral shear imaging interferometer, the technique enabled the amplitude and phase modulation of several modulation levels to be displayed simultaneously in a single interferogram. They included an imaging system which enabled simultaneously display complex modulations for several modulation levels in the same interferogram. This ability allows visually monitoring the interferogram while manually varying the optical elements that determine the input and output polarization states.

The capability to simultaneously observe a full range of amplitude and phase modulations allows one to avoid the time consuming process of polarimetric characterization together with the subsequent numerical optimization. In particular, it becomes possible to quickly identify and measure mostly-phase or mostly-amplitude TN-LCD modes of operation.

3.6. Using an interferometer

It is apparent that the phase modulation curve of an SLM can be directly measured with the aid of an interferometer. The main drawback of these kinds of systems is the high sensitivity to mechanical vibrations,

as well as the large number of optical components required. Moreover, it is also possible to study spatial phase distortions across the device aperture with interferometric methods, such as those based on the analysis of Fizeau-type fringes [57], or a Mach–Zehnder interferometer [58]. However, the Mach–Zehnder interferometer and radial shear interferometer are suitable for transmissive LC SLM only, and a digital phase-shifting interferometer incurs high cost.

Hongxin, Jian and Liying used a Twyman–Green interferometer [59] for its simple structure and easy operation, in order to evaluate the phase modulation performance of a 256 × 256 pixels reflecting liquid crystal spatial light modulator. They used both phase and intensity measurements on this single interferometer to identify the linear range of phase shift and evaluate the spatial nonuniformity of the modulator so as to obtain more accurate phase modulation. They concluded that the inherent backplane curvature of the modulator is the main contributor to phase distortion due to the modulator. Furthermore, their analysis of the root-mean-square value of the phase nonuniformity indicated that the stability of the modulator decreases with increasing grey scales. It should be noted that the other aforementioned non-interferometer-based techniques allow determining the calibration function on average for the whole device rather than for every pixel separately.

3.7. Flicker

Lizana et. al. presented a revision of diverse papers that they published about the exhaustive study of an Twisted Nematic LCoS display, they observed that the optical axis of the LCoS display molecules fluctuates as a function of the time as a consequence of the type of electrical signal addressed to the device [60]. These time fluctuations, called flicker, lead to two different physical phenomena that may decrease the efficiency when addressing diffractive elements to the display: the effective depolarization and the phase-fluctuations phenomena. They developed a study of these two phenomena and its influence on diffractive elements.

This study was done as a function of the incident angle and as a function of the wavelength, in order to detect the influence of these parameters on the effective depolarization origin and of the phase-fluctuations

The depolarized light was related to time-fluctuations of the LC molecules optical axis orientation. As the LC is an anisotropy material, time-fluctuations of the LC molecules produces changes of the reflected state of polarization as a function on the time. In particular, the type of binary signal addressed to the LCoS display was not able to keep still the molecules into a frame period, producing the time-fluctuations phenomena.

In addition, the effective depolarization (that can be larger than a 10%) detected depends on different parameters as can be the incident state of polarization, gray level addressed to the LCoS display, angle of incidence or wavelength.

Chapter 4

Phase shift assessment

As a starting point at the beginning of this chapter a computer model, that simulate the wavefront aberrations produced by the use of a reflective spatial light modulator in a branch of a Twyman-Green system under ideal conditions, is used to provide reliable fringe patterns for the quality testing of the measured phase shift. Also, some particular changes in the amplitude modulation can be analyzed.

In this model the errors introduced due to the high sensitivity to mechanical vibrations or air fluctuations of the physical system no longer exist.

In order to analyze the reliability of the moiré fringe technique to reduce the residual carrier frequency, the extraction of the phase with the moiré fringe patterns is realized.

Hence, a detailed analysis of the fringe patterns to measure the complex modulation (phase and amplitude) is possible.

4.1. Analysis

The analysis comprises the three main processes associated with the extraction of the phase by the method used for: interference, moiré fringe patterns and phase shift measurement. The interference phenomena of the optical setup are used to generate the fringe patterns due to inherent aberrations of the system. The moiré fringe patterns are usually obtained by the subtraction of two fringe patterns, in this case of the same setup, but one fringe pattern with a tilt. The phase shift measurement can be obtained using a nonlinear method. Next, each phenomena are discussed in order to provide the basics of the computer model.

4.1.1. Interference

Light is an electromagnetic wave, its propagation is a solution of the differential wave equation [61]. Any linear combination of functions that are solutions of that equation also conforms a solution. Therefore, light can be regarded as a superposition of monochromatic plane waves. When two harmonic waves are superimposed, the combined wave is the arithmetic sum of the two functions [62].

The intensity of a wave is proportional to the square of the amplitude of the electric field. In other words, the intensity resulting from the superposition of monochromatic waves is the sum of the intensities of the separate waves plus an interference term.

Interference can be made with a large number of optical setups. How-

ever, in this subsection a model of the wavefront function that describes the aberrations of a Twyman-Green interferometer is presented.

A Twyman–Green interferometer is a variant of the Michelson interferometer principally used to test optical components. The interferograms due to the primary aberrations can be described by using the wavefront function by Kingslake [63], which is given by

$$OPD = A + Bx + Cy + D(x^2 + y^2) + E(x^2 + 3y^2) + Fy(x^2 + y^2) + G(x^2 + y^2)^2$$

where the coefficients represent:

A Constant term (piston)

B Tilt about the y axis

C Tilt about the x axis

D Reference sphere change, also called defocus

E Sagital astigmatism along the y axis

F Sagital coma along the y axis

G Primary spherical aberration

This expression is designed to represent the wavefronts produced in the presence of the primary aberrations of a centered lens whose point source and image are displaced in the y direction. Thus, the wavefront is always symmetric about the y axis. The coma and astigmatism terms are referred to the Petzval surface, which is not of a great relevance in most interferograms [63]. In this wavefront model the interference pattern is simplified and the parameters due to coma, astigmatism and spherical aberration are not considered.

Here, using the computer model, the Figure 4.1.1 illustrates the simulated interferometric pattern produced by defocus.

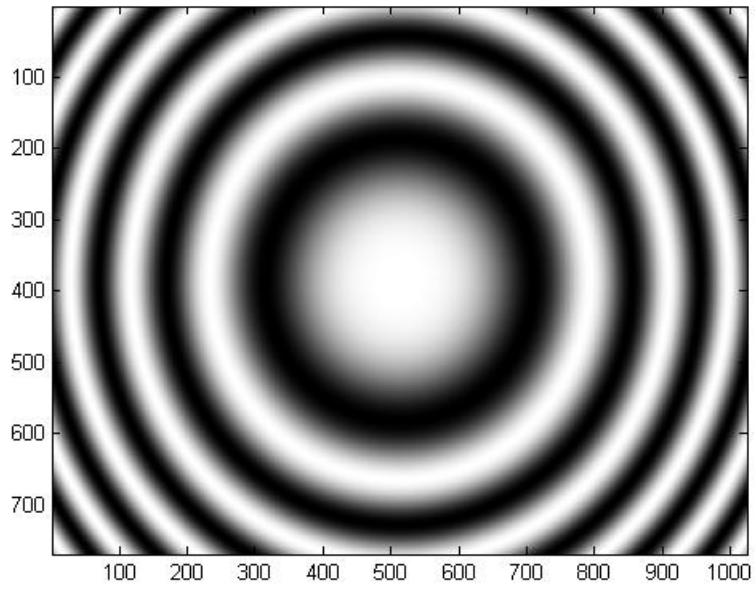

Figure 4.1.1. Simulated interferometric pattern produced by defocus aberration given for the Twyman-Green interferometer.

4.1.2. Moiré fringe patterns

This subsection deals with the use of moiré patterns in our interferometric study of the phase shift measurement. It has been shown that certain errors can be eliminated by using the moiré fringe method.

In the formation of moiré fringes there are three types of incoherent superimposition of structures: additive, subtractive and multiplicative. They correspond to three of the four basic rules of arithmetic. The optical realization and appearance of the resulting moiré pattern differ from the three types of superimposition. Knowledge of the differences is indispensable for selecting the type of superimposition for a particular application [64].

In additive superimposition, the errors due to wavefront aberrations in

the interferometer are eliminated. But there are two disadvantages in this superimposition. The moiré fringes have poor visibility and the imaging optics have to be able to resolve the carrier pattern.

In the multiplicative superimposition the structures with spatial variations in transmittance or reflectance are put in actual or virtual contact and illuminated by a light beam. The light field behind or in front of the structures is proportional, respectively, to the product of their transmittances or reflectances. This type can be also realized in the computer using logical operations [65].

Subtractive superimposition is more difficult to realize than additive and multiplicative ones. The subtraction operation is usually substituted by the absolute value difference and thus better quality fringes are obtained. This transformation also gives better visual contrast.

The moiré fringes are given by the term in which the arguments of the oscillatory function in the two interferograms are subtracted. Therefore the common elements in the two interferograms, those due to instrumental errors such as defects in the mirrors or beam splitters, are eliminated. The mathematical description of this principle was given by Yokozeki and Suzuki [66, 67, 68].

For example, subtractive superimposition of sinusoidal profile structures, I_1 and I_2 with periods d_1 and d_2 i.e. frequencies v_1 and v_2, respectively, where x represents an arbitrary point, results in intensity distribution

$$I_1(x) - I_2(x) = -sin[\pi \left(\frac{1}{d_1} + \frac{1}{d_2}\right) \mathrm{x}]\, cos[\pi \left(\frac{1}{d_1} - \frac{1}{d_2}\right) \mathrm{x}\ ]$$

$$= -sin[\pi(\nu_1+\nu_2)\ \mathrm{x}\ ]\, cos[\pi(\nu_1-\nu_2)\ \mathrm{x}\ ]$$

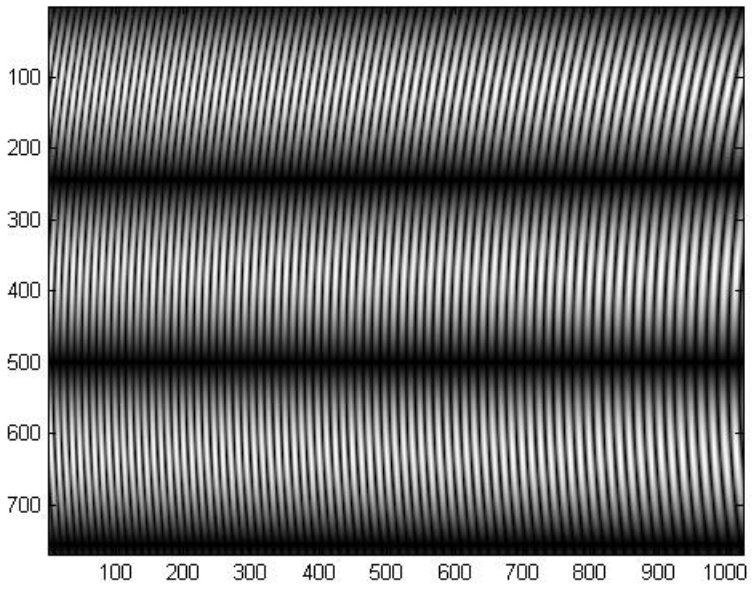

Figure 4.1.2. Simulated moiré fringe pattern produced by subtraction of two fringe patterns.

The last term $cos[\pi(\nu_1\text{-}\nu_2)\ x\ ]$ represents the moiré pattern and is readily observed provided, $v_1 - v_2 < v_{1,2}$, a condition which has to be satisfied equally in additive and multiplicative superimposition [64].

In this computer model the moiré pattern is generated by taking the absolute value of the subtraction of the intensity distribution in the first interferogram and the intensity distribution in the second interferogram (introducing a tilt). Figure 4.1.2 illustrates the simulated moiré fringe pattern produced by the subtraction of two fringe patterns. The fringe frequency of the moiré pattern increases with the magnitude of the vertical tilt applied to the second interferometric pattern.

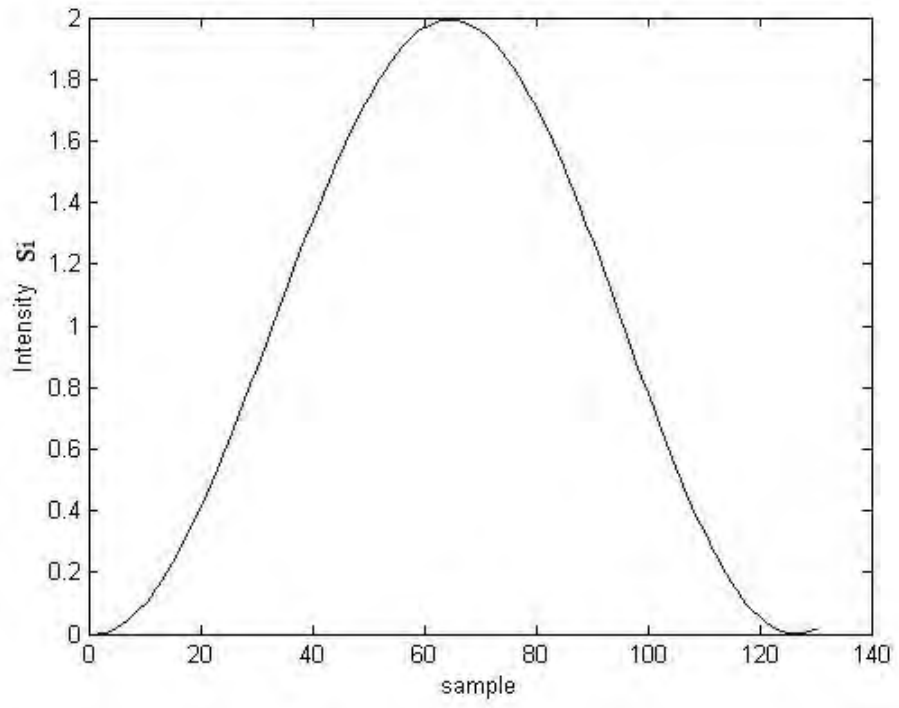

Figure 4.1.3. Function S produced by the intensities of the succession S_i of the simulated interferograms to test the phase shift.

4.1.3. Phase shift measurement method

The phase shift measurement method is based on a function S obtained from a set of intensities S_i as a part of the data acquisition of interferometric images of the interferometer configuration, in which the sensitivity and nonlinearity of the phase shifter are determined [69]. Figure 4.1.3 illustrated the function S produced by the intensity that gives the succession of simulated interferograms to testing the phase shift.

The procedure to develop the method described using fringes, require a succession of interferograms that gives the intensity across the area.

In order to obtain every S_i, two interferograms are recorded, I_{i1} and I_{i2}

$$I_{i1}(x,y) = A_{i1}(x,y) + B_{i1}(x,y)cos[\varphi(x,y)]$$
$$I_{i2}(x,y) = A_{i2}(x,y) + B_{i2}(x,y)cos[\varphi(x,y) + \delta_i(t)] \tag{4.1.1}$$

where (x, y) represents an arbitrary point;

$A(x, y)$ and $B(x, y)$ are the background and visibility functions, respectively; $\delta_i(t)$ is the increment of the phase shifting during data acquisition corresponding.

The first image, I_{i1}, is used as a reference and the second one, I_{i2}, has an unknown phase increment.

Then the average of the absolute value of the intensity differences is calculated over the full image

$$S_i = \ll \|I_{i2} - I_{i1}\| \gg \tag{4.1.2}$$

The measured intensity samples S_i do not precisely map to one complete period 2π of a sinusoidal signal. A precisely sinusoidal signal S is expected, and the acquired data points S_i are fitted into a Fourier series of sinusoids or to a sinusoidal signal in a least-squares sense [63], the fit is denoted by $\hat{S}_i$.

Finally, the error ε is minimized, ε is the sum of the squares of the differences between the measured and fitted values

$$\varepsilon = \sum_{i=0}^{N} (\hat{S}_i - S_i)^2 \tag{4.1.3}$$

To minimize Equation 4.1.3, a nonlinear algorithm like the Nelder-Mead

simplex search for slowly varying fringe density can be used [70]. Figure 4.1.4 shows the phase shifts, δ_i , calculated with the nonlinear method used.

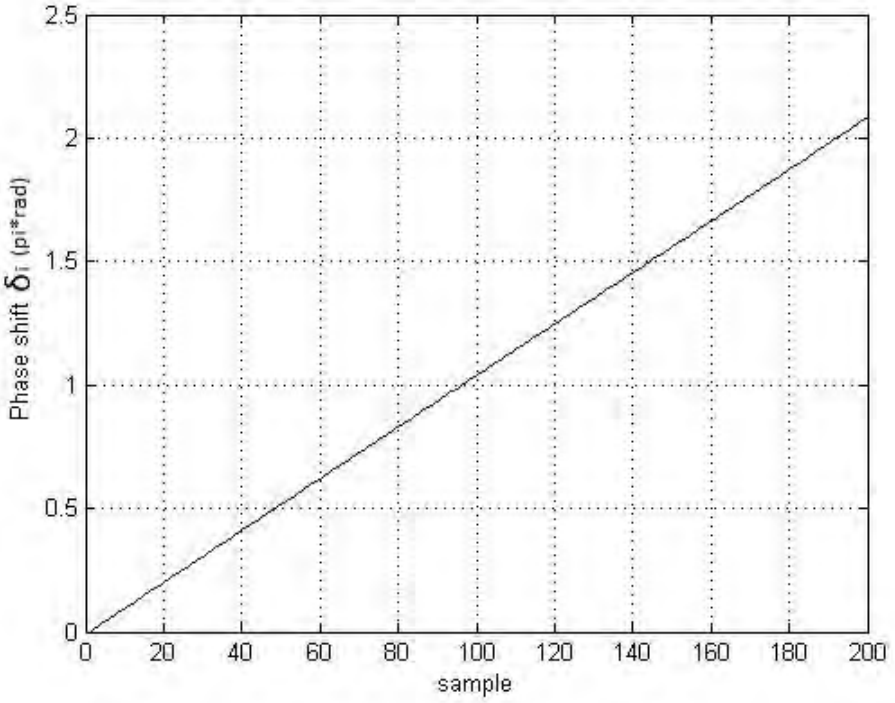

Figure 4.1.4. Shows the phase shifts, δ_i, calculated for every sample with the nonlinear method used.

For the simplicity of the technique it could be implemented in our experiment to characterize the SLM-LCoS used in the interferometer. The method was useful to find that the SLM has a limited modulation range near 1.9π of phase stroke and the response in phase to changes in the gray levels are slightly nonlinear.

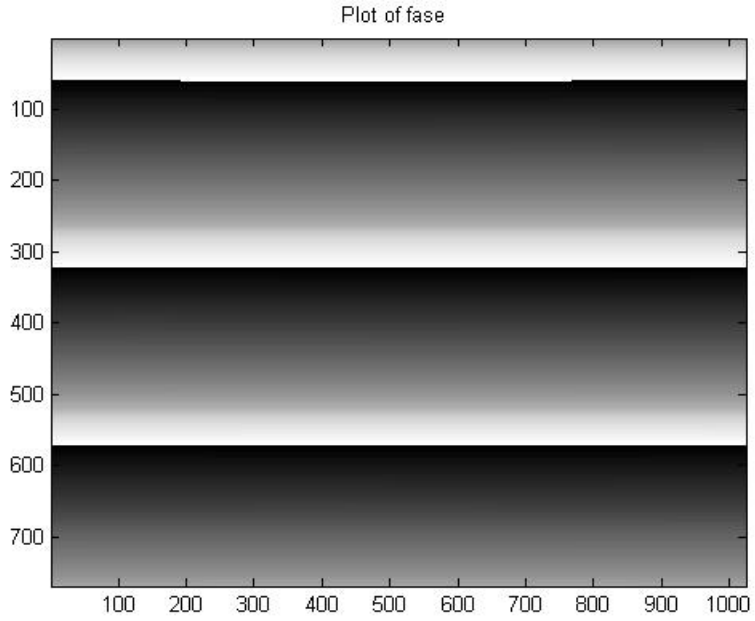

Figure 4.1.5. Phase of a moiré fringe pattern.

This analysis is complemented with the extraction of the phase of moiré fringe patterns. Figure 4.1.5 shows the phase of a moiré fringe pattern obtained by subtraction.

Chapter 5

Characterizing the SLM

This research was motivated by the interest of a method to characterize in only-phase modulation an SLM in order to be applied in diffractive optics. However, due to the molecular twist, the operating modes of a twisted-nematic liquid crystal device tend to produce a strong coupled phase-amplitude modulation [71]. Many methods that measure a single modulation level at a time and sandwich the SLM between polarization elements, as linear polarizers and retarder plates have been proposed. As such, a complete measure requires a series of time consuming sequential measurements.

In this Chapter our proposed method for establishing the complex modulation of SLMs is developed.

With this technique, the phase and the amplitude modulation can be measured simultaneously. We determined that a mostly-phase modulation with a stroke of almost 2π does not require sandwich the SLM between polarizer-analyzer, nor retarder plates, only requires a linear polarizer. The scheme polarizer-analyzer was studied also. Furthermore, the method was optimized using moiré techniques avoiding sequential measurements.

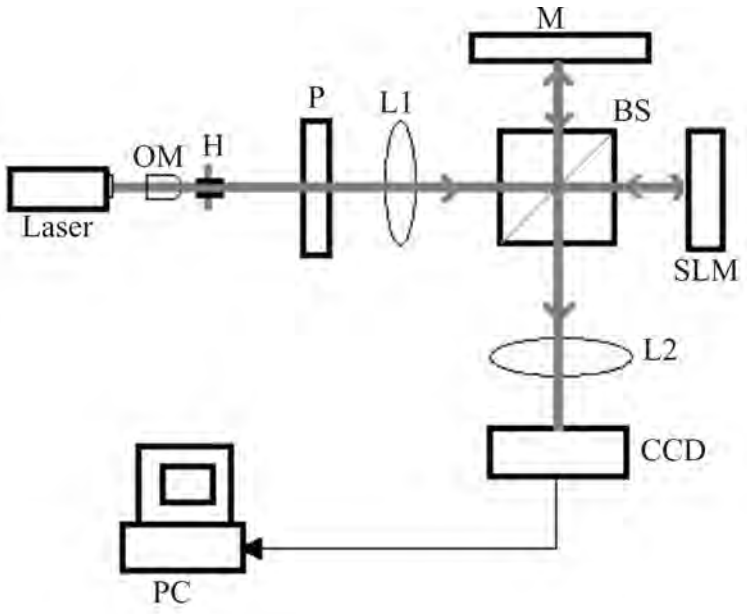

Figure 5.0.1. Setup implemented of a Twyman-Green interferometer

In this work a Michelson Interferometer type: a Twyman-Green interferometer, where one of the arms is a reflective LCoS-SLM, and the other arm is a mirror, is considered. The figure 5.0.1 shows the interferometric setup used. A laser beam, with a Gaussian spatial profile, polarized by the polarizer P is collimated by lens L1 of diameter $d = 5cm$ and focal distance $f = 10cm$. It is splitted by beam splitter BS into two beams. One beam is reflected by plane mirror M and the other beam is reflected by the LCoS-SLM. The CCD camera is located in the image plane of lens L2 to record the fringe pattern produced.

To characterize the complex amplitude response of the modulator this optical setup is capable to make measurements of the wavefront distortion of the SLM and of the optical system. The display of different gray levels on the LCoS-SLM results in a phase shift appearing in the interference pattern,

a fringing which is used to test in phase the SLM by measuring a sequence of intensities using algorithms of phase shift errors. This data acquired of the process due to fringe patterns changes when the gray level displayed changes generating a sinusoidal function. Which is fitted to a sinusoidal function, the sum of the squares of the differences between the measured and fitted values give the error ε to be minimized.

Next, let us explain the experimental process that we have followed in order to determine the complex modulation of an SLM using a polarizer only and a polarizer-analyzer couple in the setup.

5.1. Experimental fringe patterns

The experimental fringe patterns were obtained for different polarization schemes and displaying gray levels in the SLM, this method assumes that modulation is equal over all the SLM.

Consider the Twyman Green interferometer described in Figure 5.0.1 with the linear polarizer at a fixed angle.

The interference intensity considered for this interferometer is given by the equation

$$I_0(x,y) = I_R(x,y) + I_{L0}(x,y) + 2\sqrt{I_R(x,y)I_{L0}(x,y)}cos[2\pi\ (ax+by) + \varphi(x,y)] \tag{5.1.1}$$

where (x,y) represents an arbitrary point; $\varphi(x,y)$ is the phase difference between the reference mirror and the LCoS-SLM, $I_R(x,y)$ is the intensity of the beam reflected by the mirror and $I_{L0}(x,y)$ is the intensity of the beam

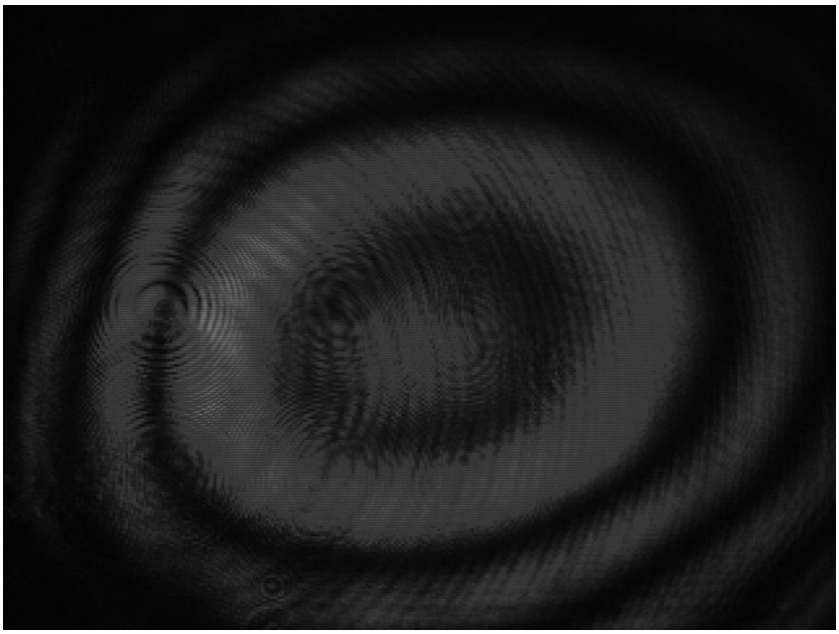

Figure 5.1.1. Fringe pattern I_0 produced by the implemented interferometer displaying the gray level zero on the SLM.

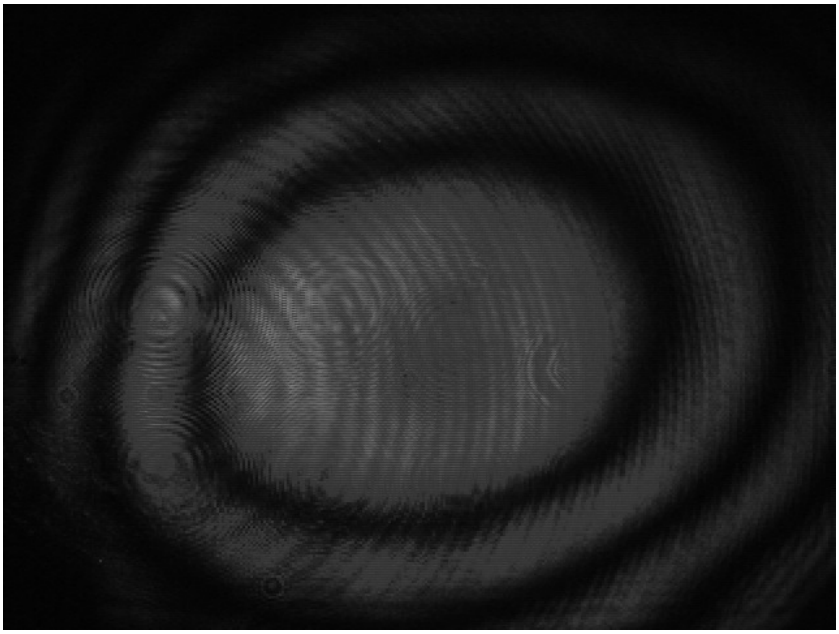

Figure 5.1.2. Fringe pattern I_N produced by the implemented interferometer displaying a gray level N on the SLM.

reflected by the LCoS, a and b are the carrier coefficients which allow to address displacements in the x and y directions. The term $\varphi(x, y)$ holds the aberrations of the optical components and the LCoS-SLM itself. Note that $I_0(x, y)$ could not have straight lines unless $\varphi(x, y) = 0$, that is, unless all the optical components have high optical quality with negligible aberrations.

The phase and amplitude variations that an electrically addressed SLM introduces to a light beam impinging on it depend on the electrical voltage introduced to the liquid crystal. These voltages are related to the gray level displayed on the SLM. If display on the LCoS-SLM a digital image, $g(x, y)$ containing a gray level $N \leq 255$, the interference equation is expressed by

$$\begin{aligned} I_N(x, y) = I_R(x, y) + I_{LN}(x, y) + 2\sqrt{I_R(x, y) I_{LN}(x, y)} * \\ cos[2\pi\ (ax + by + cy) + \varphi(x, y) + G_N(x, y)] \end{aligned} \tag{5.1.2}$$

where (x, y) represents an arbitrary point; $G_N(x, y)$ is the phase difference (See figure 5.1.2) and $I_{LN}(x, y)$ is the amplitude function introduced by the image function $g(x, y)$, and c is a small carrier coefficient in the y direction introduced manually. The purpose of the inclusion of the second carrier term $2\pi cy$ is related to the generation of moiré fringe patterns.

Figure 5.1.1 shows the fringe pattern I_0 produced by the implemented interferometer displaying the gray level zero on the SLM and the figure 5.1.2 shows a fringe pattern I_N produced by displaying a gray level N on the SLM. Notice that there is a phase difference between the interferograms of I_0 and I_N.

Figure 5.1.3 shows fringe patterns produced with a carrier.

a) 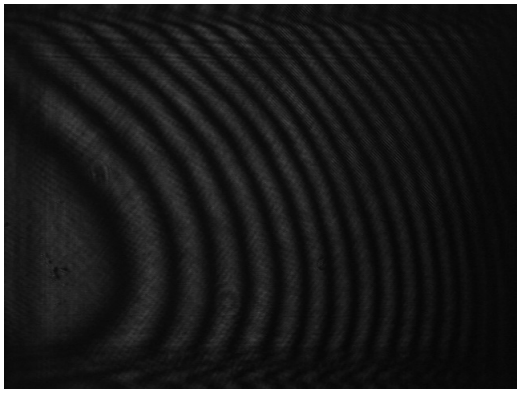 b) 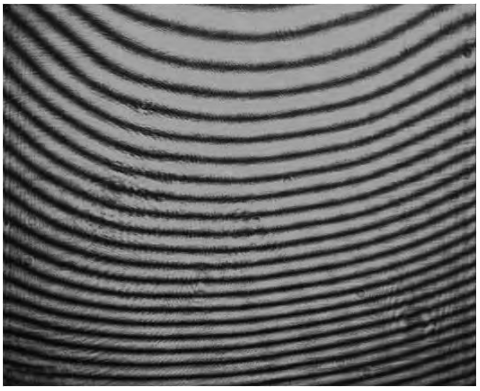

Figure 5.1.3. Fringe patterns produced by applying a tilt to the mirror, a) carrier is in the x direction and b) carrier is in the y direction.

In order to get the amplitude modulation A without the Gaussian beam profile, two operations must be realized; the intensity subtraction $I_S(x,y) = I_N(x,y) - I_0(x,y)$ and the mean $A = \ll I_S(x,y) \gg$.

5.1.1. The use of a single polarizer

The interferometric setup is as shown in Figure 5.0.1, an unpolarized laser beam at $\lambda = 632.8nm$ is collimated using a positive lens L1. It propagates through polarizer P. To acquire the interference fringes a commercial reflective TN-LCD-based SLM, LCR-2500 (LCoS-SLM) from Holoeye has been used as SLM. It poses a display resolution of 1024 x 768 pixels with a pixel-pitch of 19μm x 19μm. The voltage with a total of 256 levels on every pixel can be modulated separately [13]. The LCoS-SLM is addressable and programmable by a personal computer PC, the images are recorded with a CCD that poses a resolution of 640 x 480 pixels. Instead of a randomly polarized light it can be used circularly polarized light to illuminate the polarizer P; also, linearly polarized light can be used but then the polarizer P

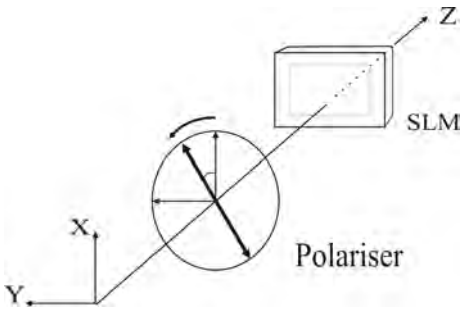

Figure 5.1.4. Diagram showing the coordinate system used.

must be replaced by a half wave plate. Figure 5.1.4 shows the right handed coordinate system used. The polarizer direction was measured from the laboratory vertical axis. In this study the polarizer was turned from 0° to 175° with increments of 5° but we only present the results of the best polarization squeme.

As mentioned before, the display of different gray levels in the LCoS-SLM results in a phase shift appearing in the interference pattern, a fringing which is used to test in phase the LCoS-SLM by measuring a sequence of intensities S_i. This data sequence was acquired of the process due to fringe patterns change when the gray level displayed changes, generating a sinusoidal function S. The figure 5.1.5 shows the sinusoidal function S obtained by 256 gray levels displayed on the LCoS-SLM for the polarizer turned to 168°.

The best scheme for mostly-phase and minimum amplitude modulation was obtained with the polarizer turned to 168°. Figure 5.1.6 shows the corresponding phase displacement, with a stroke of almost 2π, calculated using the nonlinear method of Section 4.1.3. The intensities S_i were obtained displaying constant images of every gray level on the LCoS-SLM and for the

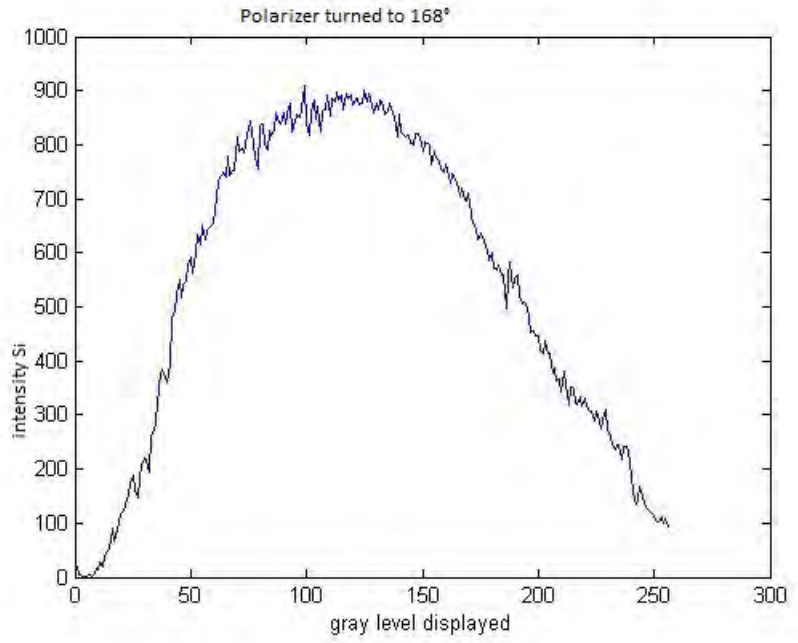

Figure 5.1.5. Function S obtained with the intensities S_i measured of gray levels displayed on the LCoS-SLM for the polarizer turned to 168°.

polarizer turned to 168°. It can be noticed the nonlinearity of the LCoS-SLM in phase.

Figure 5.1.7 shows the amplitude modulation measured for every gray level displayed on the LCoS-SLM with the polarizer turned to 168°. It can be noticed the nonlinearity of the LCoS-SLM in amplitude.

It is important to mention that using a single polarizer (without using analyzer) we observed a mostly-phase modulation with minimum amplitude modulation.

5.1.2. The use of a polarizer-analyzer couple

The interferometric setup used for the scheme polarizer-analyzer couple was the same as shown in Figure 5.0.1 but additionally an analyzer was

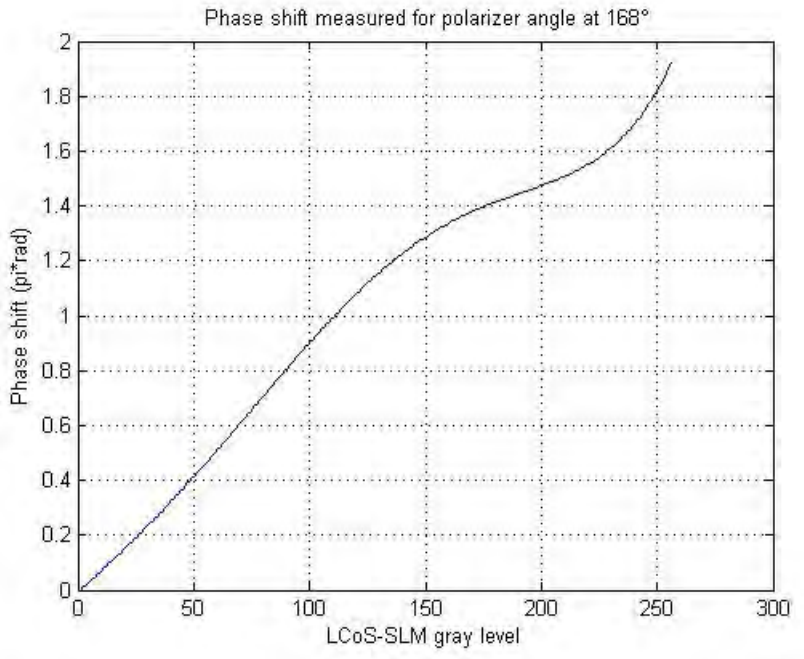

Figure 5.1.6. Phase modulation measured using a nonlinear method.

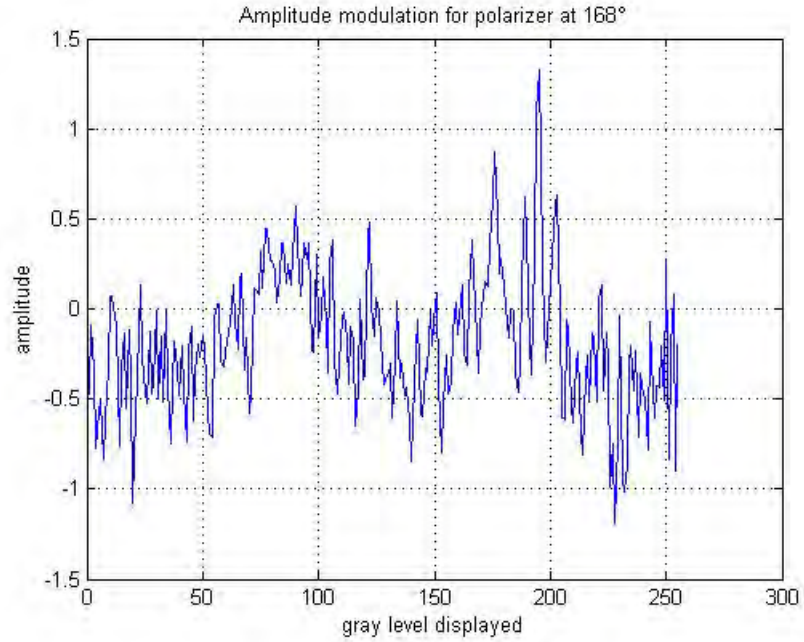

Figure 5.1.7. Shows the amplitude modulation obtained for *every* gray level displayed on the LCoS-SLM with the polarizer turned to 168°.

located in front of lens L2. So an unpolarized laser beam at $\lambda = 632.8nm$ was collimated using a positive lens L1. It propagated through polarizer P. Then the beam was splitted by beam splitter BS into two beams. One beam was reflected by mirror M and the other beam was reflected by the LCoS-SLM. A CCD camera that poses a resolution of 640 x 480 pixels was located in the image plane of lens L2 to record the fringe pattern produced. The coordinate system used for the analyzer was the same used in the section 5.1.1 (see figure 5.1.4). The analyzer direction was measured from the laboratory vertical axis also.

As mentioned before, the display of different gray levels in the LCoS-SLM results in a phase shift appearing in the interference pattern, a fringing which is used to test in phase the LCoS-SLM by measuring a sequence of intensities and this data sequence was acquired of the process due to fringe patterns change when the gray level displayed changes, generating a sinusoidal function. For this the polarizer angle was fixed and the analyzer angle was turned.

Figure 5.1.8 shows the sinusoidal function S obtained for the gray levels displayed on the LCoS-SLM for the polarizer turned to 30° and analyzer turned to 150°.

Figure 5.1.9 shows the amplitude modulation measured for the gray levels displayed on the LCoS-SLM with the polarizer turned to 30° and analyzer turned to 150°.

It is important to mention that in the scheme polarizer-analyzer couple we observed that the amplitude modulation increased a lot but the phase modulation decreased little.

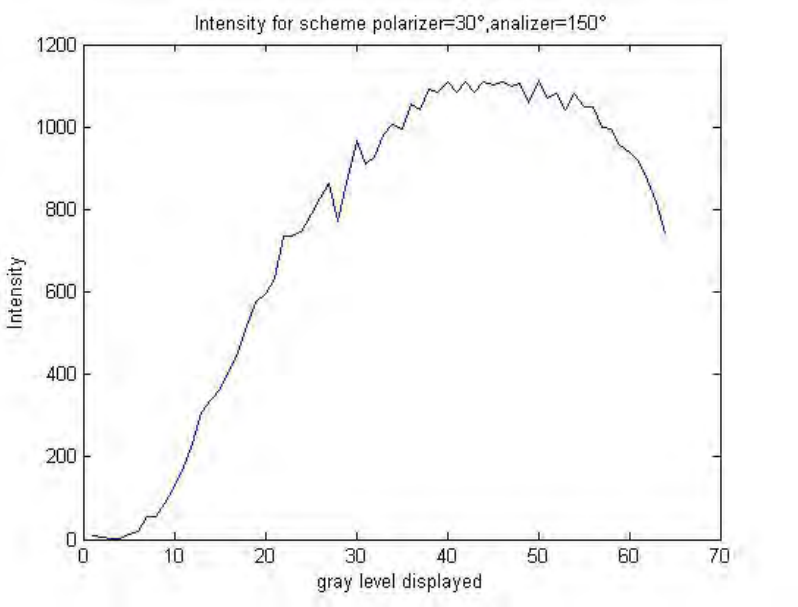

Figure 5.1.8. Shows the sinusoidal function S obtained by the gray levels displayed in the LCoS-SLM with the polarizer turned to 30° and analizer turned to 150°.

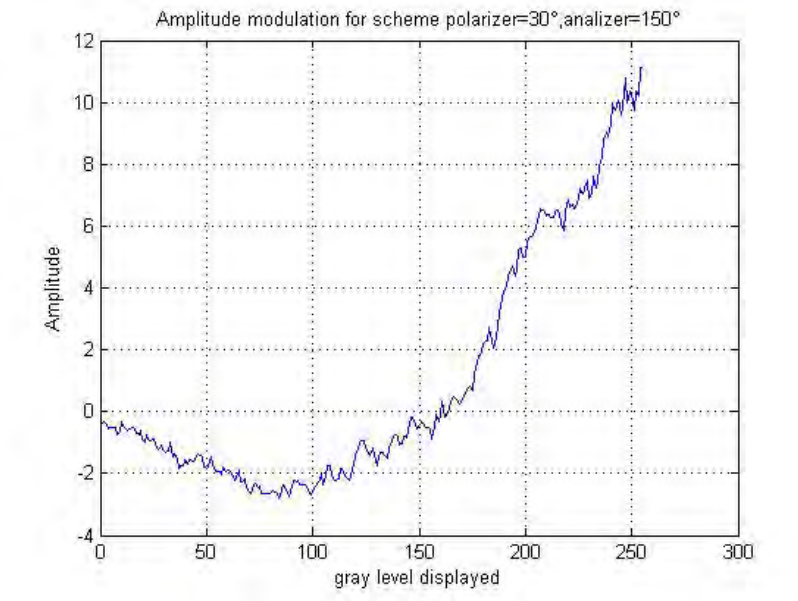

Figure 5.1.9. Shows the amplitude modulation obtained for *every* gray level displayed in the LCoS-SLM with the polarizer turned to 30° and analizer turned to 150°.

5.2. Optimization

The optimization procedure consists basically of a heuristic approach introducing carrier fringes and forming a moiré pattern that subtract the aberrations of the optical system. The moiré patterns are needed to examine the phase variations of the LCoS-SLM but the analysis of the amplitude does not require it.

5.2.1. Moiré technique

For the experimental demonstration of the usefulness of moiré patterns to visualize the phase modulation introduced by an SLM is used the simple optical setup of Figure 5.0.1 but more complicated schemes could be used as well, like the one proposed by Yamaguchi, et. al. [72] which is an interferometric set up to measure the amplitude and phase of an LCTV with linear polarizers and quarter-wave retarders.

The subtractive superimposition of Equation 5.1.1 and Equation 5.1.2 results in intensity distribution

$$I_s(x,y) = DC(x,y) + H(x,y) + 2I_R(x,y)\sqrt{I_0(x,y)I_{LN}(x,y)}cos[2\pi\ cy + G_N(x,y)] \tag{5.2.1}$$

or the typical equation containing the moiré patterns

$$I_s(x,y) = DC(x,y) + H(x,y) + m(x,y) \tag{5.2.2}$$

where $DC(x,y)$ is the background amplitude, $H(x,y)$ represents high frequency fringes and $m(x,y)$ represents the moiré pattern.

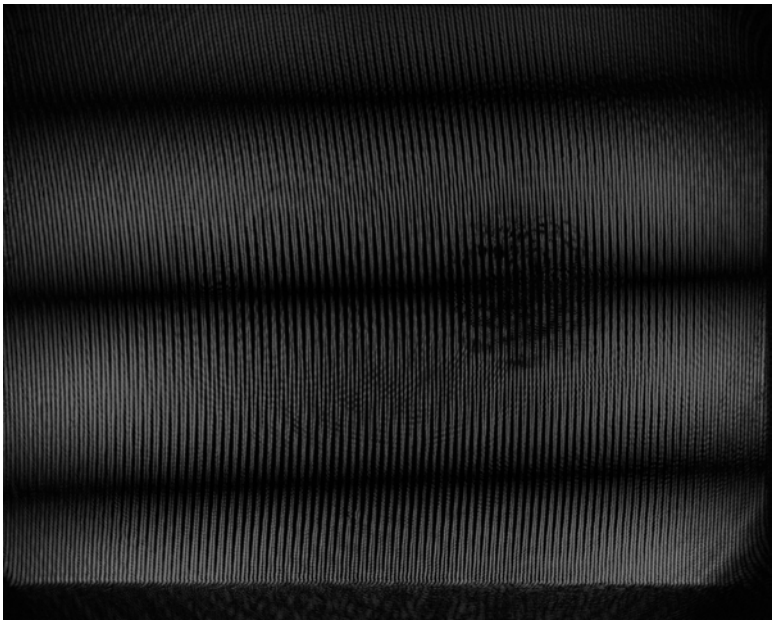

Figure 5.2.1. Subtractive moiré fringe pattern formed by two interferograms displaying the gray level zero on the LCoS-SLM for both of them.

Figure 5.2.1 shows a subtractive moiré fringe pattern formed by two interferograms displaying the image of constant gray level zero on the LCoS-SLM for both interferograms.

The moiré term $m(x, y)$ contains the phase modulation $G_N(x, y)$ plus some horizontal fringes whose frequency depends on coefficient carrier c. Notice that under the subtractive operation, the undesired term that contains the aberrations $\varphi(x, y)$ has been eliminated.

As mentioned in subsection 4.1.2, due to the background term $DC(x, y)$ that appears in Equation 5.2.2, to improve the moiré fringes contrast, the complex images must be obtained by taking the absolute value of the subtraction of intensities $I_N(x, y)$ and $I_0(x, y)$.

To observe the phase modulation in the SLM we constructed the digital

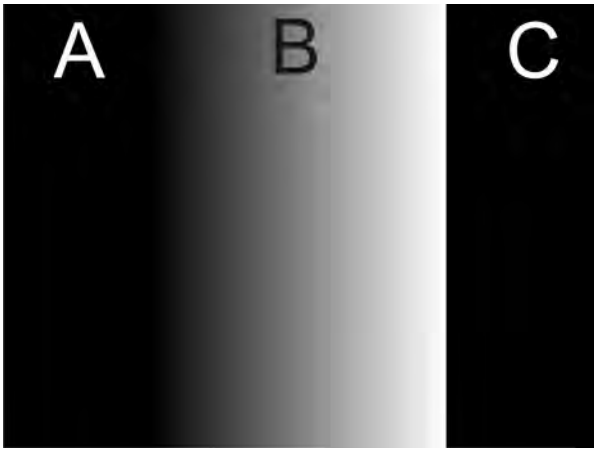

Figure 5.2.2. Image $g1(x, y)$ displayed on the LCoS-SLM.

image $g1(x, y)$ to display it in the LCoS-SLM, figure 5.2.2, by dividing the image in three rectangular sections denoted from left to right as A, B and C. Where$A$ and C rectangles are black, i.e., the constant gray level (GL) equal to zero, and the central one, B, is a ramp of vertical equally spaced gray levels increasing monotonically from $N = 0$ to $N = 255$.

With this image displayed the moiré pattern fringe remained the horizontal fringes straight in section A and C but deformed in section B. If the relation between GL and $G_N(x, y)$ would be linear we expected to visualize also a linear fringe deformation in B, but the fringe deformation is slightly nonlinear.

With the previous procedure for moire fringes, the incident polarization on the LCoS-SLM can be changed to observe in real time the phase modulation. In this way the moiré patterns show the phase variations of the LCoS-SLM by observing the deformation of the straight fringes as a function of the gray levels displayed in the LCoS-SLM. The maximum phase

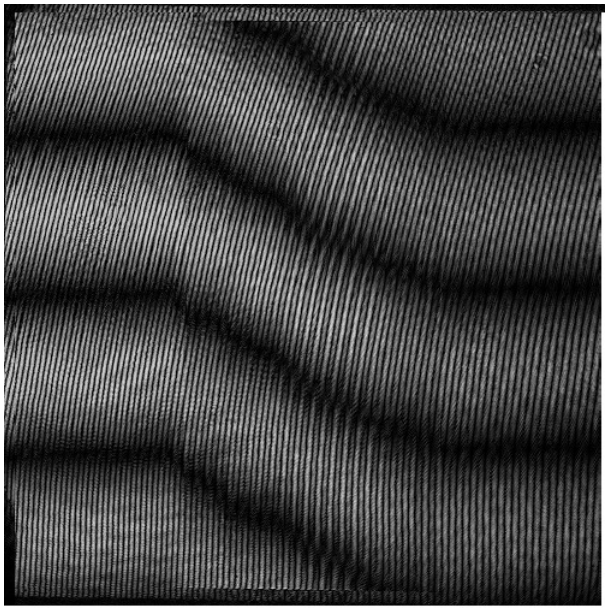

Figure 5.2.3. Moiré fringe pattern formed by displaying the image $g1(x, y)$ on the LCoS-SLM, for the polarizer turned to 168°.

stroke could be observed by analyzing the shift of the fringes on the frontier between sections B and C.

By performing those operations it was simple to visualize immediately the effect of the phase modulation introduced by the LCoS-SLM by rotating the polarizer. Furthermore, a quantitative measurement of the phase shift $G_N(x, y)$ between $I_0(x, y)$ and $I_N(x, y)$ can be found by using $c = 0$ and applying the algorithm proposed in Section 4.1.3.

Figure 5.2.4 shows the moiré fringe pattern formed by displaying the image $g1(x, y)$ on the LCOS-SLM and shows the nonlinear fringe deformation in B, for the polarizer turned to 168°, i.e. for maximum phase modulation.

Figure 5.2.3 shows the moiré fringe pattern formed by displaying the

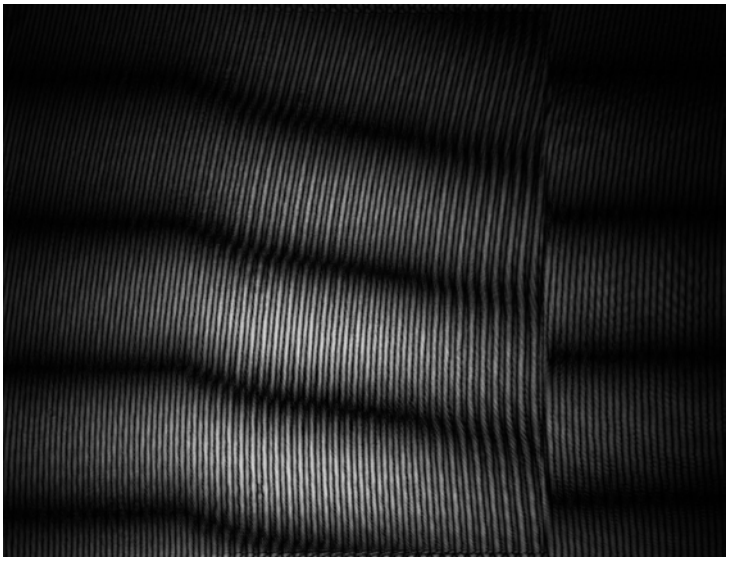

Figure 5.2.4. Moiré fringe pattern formed by displaying the image $g1(x, y)$ on the LCoS-SLM for the polarizer turned to 135°.

image $g1(x, y)$ on the LCoS-SLM and shows the the shift of the fringes on the frontier between sections B and C, for the polarizer turned to 135°.

Chapter 6

Flicker behavior in a TN LCoS-SLM

Twisted-Nematic (TN) Liquid Crystal on Silicon (LCoS) Spatial Light Modulators (SLMs) are widely used for their capability to control beams. However, Lizana et. al. [73] observed that the optical axis of the LCoS display molecules fluctuates as a function of the time as a consequence of the type of electrical signal applied to the device.

These time fluctuations lead to two different physical phenomena that may decrease the efficiency when addressing diffractive elements to the display: the effective depolarization and the phase-fluctuations phenomena. It is then necessary to understand these fluctuations [74], a phenomenon also known as flicker [75], and the means to mitigate them.

The flicker has been observed either as high frequency variations of polarization, attenuation or high phase fluctuations on the wave front modulated by the LCoS device.

This Chapter presents some evaluation of the flicker behavior for different polarization schemes and temperatures, the quantitative evaluation

shown that flicker is effectively reduced only under low temperatures but also its phase modulation range decreases.

6.1. Flicker assessment

We studied the flicker behavior in a twisted nematic LCoS-SLM for different polarization schemes and temperatures. The quantitative evaluation showed that flicker is effectively reduced only by cooling the LCoS-SLM panel to temperatures just below 0°C but the LCoS-SLM modulation range is also affected [76].

6.1.1. Flicker measurement method

In order to measure the flicker we used a Twyman-Green interferometer with an LCoS-SLM in one arm and a high quality mirror in the second arm. The mirror was aligned by means of a precision gimbal mount. The beam from a linearly polarized laser of $\lambda = 632.8nm$ was collimated using a positive lens and filtered using a spatial filter. A diaphragm limited the diameter of the expanded beam to the height of the LCoS-SLM display. A beam splitter with an uncoated second surface was used. Phase fluctuations due to LCoS electric polarization are not evident to the naked eye, as they occur at a frequency of 120 Hz. Therefore, a high-speed CCD camera was used to capture the temporal evolution of the interferogram. We selected a slightly wedged beam splitter aligned to the vertical axis. Therefore, the reflections from the uncoated surface induce high frequency vertical fringes that are not visible to the naked eye, but are registered by the high-speed CCD. We adjusted the

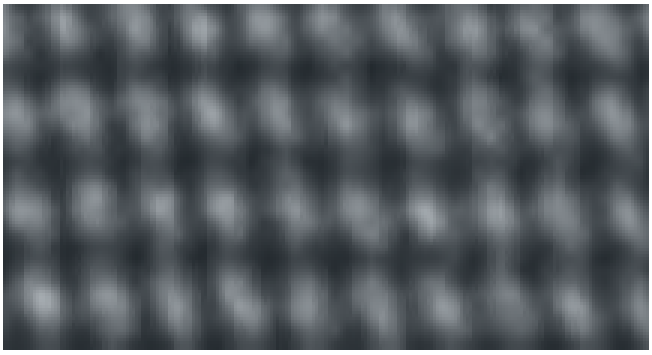

Figure 6.1.1. Pattern of bright spots periodically arranged, used to measure the flicker.

tilt of the reference mirror to introduce horizontal fringes of approximately the same spatial frequency as those due to the beam splitter. The resulting interferogram was a pattern of bright spots periodically arranged, as shown in the Figure 6.1.1.

When the optical length of one arm of the interferometer is modified the effect is observed as the vertical displacement of the spots. Therefore, by tracking the spatial position of the spots at each frame of the high speed video, we were able to quantify the time evolution of the phase. We quantified the phase fluctuation averaging the displacement of several spots at each frame recorded and calculating the RMS value [82].

6.1.2. Cooling process

As mentioned in [82] cooling LCoS-SLM is a known procedure and has been used to avoid damages caused by high power lasers or when the device is deployed in a hot environment. In low optical power applications, the heat generated by the LCoS can be dissipated by natural convection.

The manufacturer reports that the internal panel temperature increases

about 10°C to 35°C. The change in viscosity, and thus flicker, due to this temperature increment is not noticeable.

For cooling the LCoS-SLM we have used a device based on a Peltier cooler to chill the LCoS panel. Three basic elements act as a detector and actuators in this device; the first is a thermostat that reads the temperature in the LCoS' panel housing. The panel and its housing have a thermal contact extended also to the second element, the Peltier-tip/tilt circulator mount. The peltier was used with operating maximal current and voltage of 6 A and 15.7 V.

The setup implemented, a Twyman-Green interferometer, is highly sensitive to mechanical vibrations. And the water circulation in the cooling circulator disturbs the mechanical stability required to carry on flicker measurements. Then, the control stage used in the cooling system must adjust only the peltier temperature during the measurement time with the water circulator switched off. Once the measurements have been made, the water circulator is switched on again to evacuate the exceeding heat from the lower face of the peltier device.

6.2. Measurement in a polarization scheme

From the optical point of view, the depolarization effect in the LCoS-SLM is caused by temporal fluctuations of the state of polarization of the reflected beam, originated from fluctuations of the liquid crystal (LC) molecular orientation as a function of time [77, 78] and a limited viscosity of the LC molecules [74]. Depolarization also depends on wavelength; the shorter the wavelength the larger depolarization exhibits the LCoS [78]. Measurements to obtain an intensity modulation response of twisted nematic SLM by Mueller matrix for the visible spectral range has also been studied [79]. The use of a Poincaré-sphere representation has been proposed to understand changes in polarization in twisted nematic LC displays [80]. Finally, phase fluctuations in PALCoS displays have been characterized for different pulse width modulation (PWM) addressing schemes [81].

In this work three different input polarization states to the LCoS were studied. First, we studied a scheme of linear vertical polarization. Second, we studied a scheme that minimizes flicker modulation. Finally, we studied a scheme that maximizes phase modulation.

It has been shown [82] that the reduction of flicker attains an almost asymptotic behavior at -5 °C, then for the experiments carried out in this work we have only considered two temperatures, the room temperature (at 23 °C) and the low temperature (at -5 °C). Only the gray levels: 0, 130, 200, and 255 were considered in the measurements of flicker intensity.

Next, the responses to these input polarizations (at two given temperatures 23°C and at -5°C) are discussed and show that the calibration of the

input polarization state is important to decrease phase flicker when combined with a thermal control process.

The step from 0 to 30 gray levels in the figures of phase range dynamic was attributed to a miscalibration between the electronic driver and the replaced LC display used.

6.2.1. Scheme of linear vertical polarization

A scheme of linear vertical polarization was studied in the phase dynamic range and in the flicker modulation. In figure 6.2.1 it can be seen that phase modulation is lower nearly 7% for temperature at -5°C than for temperature at 23°C.

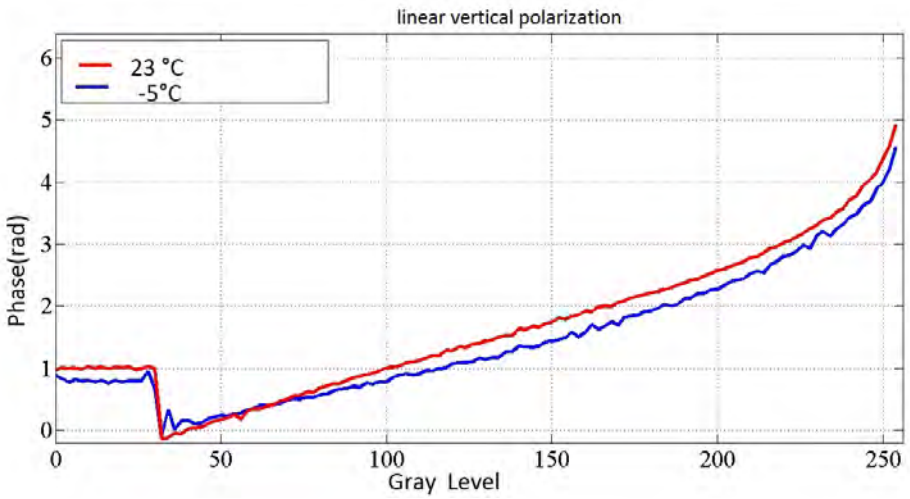

Figure 6.2.1. Phase modulation as a function of the gray level displayed on the LCoS-SLM at temperatures of 23°C and -5°C. Using the scheme of linear vertical polarization.

Table 6.1 shows the quantitative values of flicker measured as a function of the gray level displayed on the SLM for temperatures at 23°C and at -5°C.

Gray level	23°C	-5°C
0	12.09	6.69
130	19.612	7.628
200	14.798	7.314
255	7.99	7.039

Table 6.1. Measured flicker (in degrees) of some gray levels at a temperature of 23°C and at -5°C using the scheme of linear vertical polarization.

The figure 6.2.2 shows the measured flicker (in degrees) of some gray levels at a temperature of 23°C and at -5°C using the scheme of linear vertical polarization.

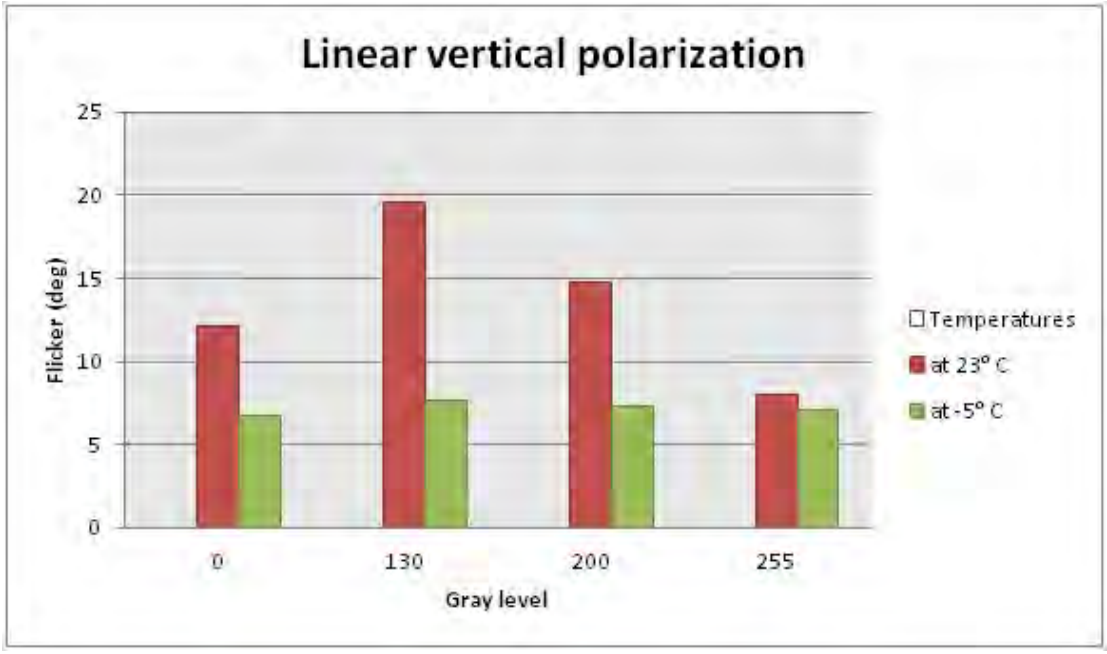

Figure 6.2.2. Measured flicker as function of the gray level displayed on the LCoS-SLM at temperatures of 23°C and -5°C. Using the scheme of linear vertical polarization.

6.2.2. Scheme that minimizes flicker modulation

Our main interest was to find an optimum incident polarization state able to provide both, maximum phase modulation and the minimum flicker modulation. To calculate the Stokes parameters that let us find an optimum incident polarization state able to cancel the effects of flicker into the LCoS device we proceeded according to the method proposed in [83]. In this study we found a scheme that minimizes the flicker modulation but the phase dynamic range decreased also, see figure 6.2.3.

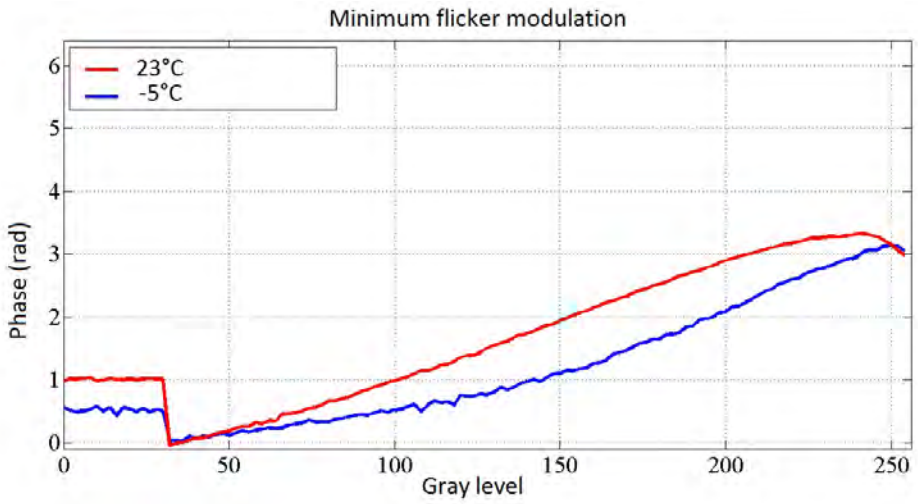

Figure 6.2.3. Phase modulation as a function of the gray level displayed on the LCoS-SLM, at a temperature of 23°C and at -5°C. Using the input polarization state that minimizes the flicker.

Table 6.2 shows the quantitative values of flicker in the figure 6.2.4 as a function of the gray level displayed on the SLM for temperatures at 23°C and at -5°C.

a)

Gray level	temperature at 23°C			
	series 1	series 2	series 3	series 4
0	13.067	13.095	11.843	11.896
130	22.272	22.435	20.798	21.914
200	17.399	17.01	19.416	19.131
255	2.922	3.434	2.807	3.406

b)

Gray level	temperature at -5°C			
	series 1	series 2	series 3	series 4
0	2.989	3.633	3.131	4.653
130	3.742	5.236	3.99	5.156
200	5.046	6.136	5.419	6.136
255	2.015	4.129	2.835	4.129

Table 6.2. Measured flicker (in degrees) of gray levels at a temperature of a) $23°C$ and b) $-5°C$ using the input polarization state that minimizes the flicker.

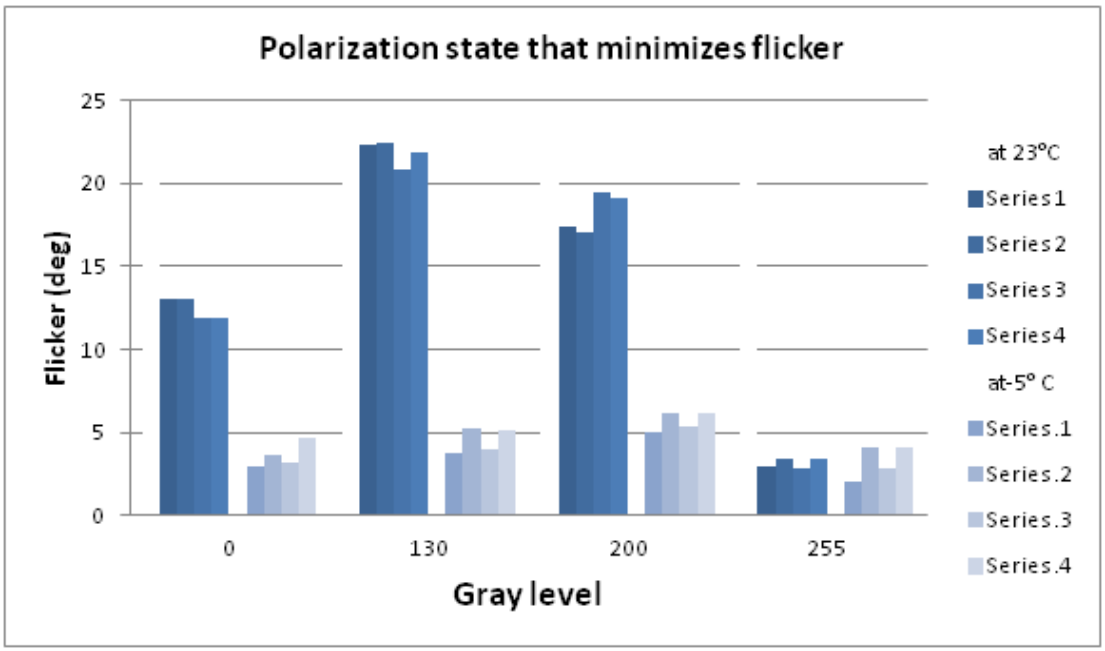

Figure 6.2.4. Measured flicker as a function of the gray level displayed on the LCoS-SLM, at a temperature of $23°C$ and at $-5°C$. Using the input polarization state that minimizes the flicker.

Flicker intensity does not behave uniformly within the whole gray level at 23°C, as can be seen in figure 6.2.4. Furthermore, we found that is just in this configuration that flicker intensity reduces almost homogeneously at 4 degrees and there is not a same optimum incident Stokes vector for all the gray levels studied.

In this scheme, 4 series of measurements for both temperatures were realized, in this way we can observe in our experiment the repeatability of the measured values.

6.2.3. Scheme that maximizes phase modulation

As mentioned before, our main interest was to find an optimum incident polarization state able to provide both, maximum phase modulation and the minimum flicker intensity.

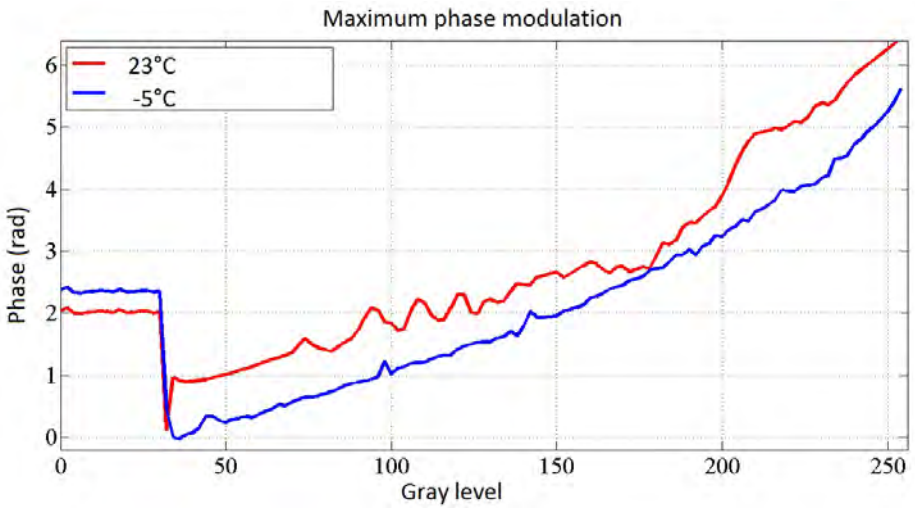

Figure 6.2.5. Phase modulation as a function of the gray level displayed on the LCoS-SLM at a temperature of $23°C$ and at $-5°C$, using the input polarization state that maximizes the phase modulation.

For applications in interferometry, we calculate the incident polarization state that let us find an optimum phase modulation of almost 2π when using a laser at 632 nm of wavelength. We proceeded according to the method proposed in [84]. This state was obtained using only a linear polarizer turned to 170°C with the coordinate system used in Chapter 5.

In this study we found a scheme that maximizes the phase dynamic range but the flicker intensity increased also at 23°C. Figure 6.2.5 shows the phase modulation as a function of the gray level displayed on the LCoS-SLM at a temperature of 23°C and at -5°C, using the input polarization state that maximizes the phase modulation.

Table 6.3 shows the quantitative values of flicker intensity plotted in figure 6.2.6 as a function of the gray level displayed on the SLM for temperatures at 23°C and at -5°C.

a)

Gray level	temperature at 23° C			
	series 1	series 2	series 3	series 4
0	12.5	12.503	12.72	12.802
130	22.23	22.359	22.52	22.58
200	29.553	28.862	28.832	28.857
255	7.034	7.397	7.229	7.336

b)

Gray level	temperature at -5° C			
	series 1	series 2	series 3	series 4
0	1.902	1.885	1.963	1.952
130	3.25	3.374	3.307	3.361
200	5.411	5.687	5.619	5.613
255	1.78	1.674	1.584	1.675

Table 6.3. Measured flicker (in degrees) of gray levels at a temperature of a) 23°C and b) -5°C. Using the input polarization state that maximizes the phase modulation.

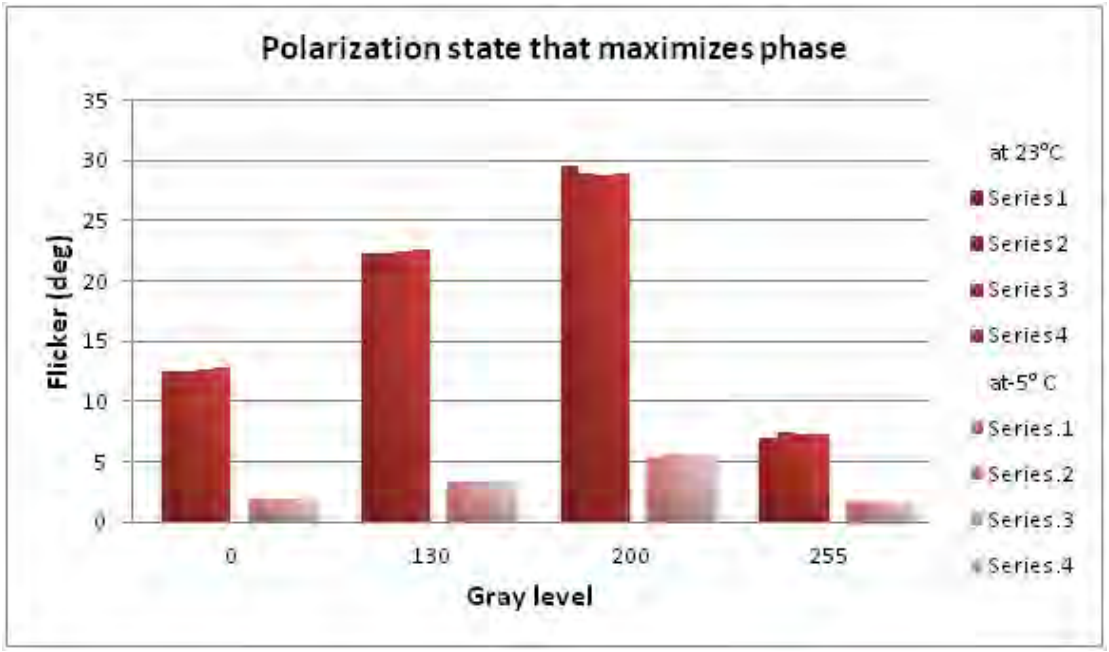

Figure 6.2.6. Measured flicker as a function of the gray level displayed on the LCoS-SLM at a temperature of $23°$C and at $-5°$C. Using the input polarization state that maximizes the phase modulation.

Flicker intensity does not behave uniformly within the whole gray level at 23°C, and the flicker intensity increased at this temperature in respect of that measured in the last scheme, as can be seen in figure 6.2.6. Four series of measurements for both temperatures were realized, in this way we can observe in our experiment the repeatability of the measured values. Furthermore, we found that is just in this configuration that flicker intensity reduces almost homogeneously at a mean flicker value around 3 degrees.

Chapter 7

Conclusions

We have demonstrated a new technique to measure the complex modulation of a spatial light modulator based on a Twyman-Green interferometer with imaging. In this work, we have found the incident polarization state that enables the maximum phase modulation with a minimum amplitude modulation, i.e. a mostly-phase operating mode. This was achieved using only a polarizer without using an analyzer, or retarder plates. Furthermore, the amplitude modulation can be increased using the analyzer also. We applied a nonlinear method to the measurement of phase modulation in the SLM device.

The distinctive feature of the proposed moiré technique is its ability to visualize the operation of gray levels instantaneously. This feature allows an optimization of operating modes of polarization, without the need for a polarimetric characterization and numerical optimization of input and output polarizations. This tremendously reduces the effort needed to test and optimize the performance of a modulator under alternative configurations, particularly of the twisted nematic liquid crystal type. Direct observation

of phase modulation curves permitted a quick manual optimization of the input polarization states leading to a mostly–phase operating mode.

Fluctuations in phase and amplitude, known as flicker, appeared in the LCoS-SLM. We found that there is not the same optimum incident Stokes vector for all the gray levels related to the different polarization schemes used by the LCoS-SLM itself, i.e. the flicker intensity response varies with the gray level displayed on the LCoS-SLM. The frequency variation of these fluctuations can be reduced only by thermal methods; but the LCoS-SLM modulation capability is also affected, which means that the increase in the liquid crystal molecules viscosity is what is mainly responsible for flicker reduction. Using a polarimetric method a low temperature, flicker can be further reduced by a small amount, but this reduces the phase dynamic range.

The main results of this work have been published in references [76, 84].

Bibliography

[1] J. W. Goodman, Introduction to Fourier Optics, Roberts and Company Publishers, Englewood, Colorado, 3rd ed., 2005.

[2] Data sheet Laser 2000, Spatial Light Modulators, 2009.

[3] G. D. Love. Wave-front correction and production of zernike modes with a liquid-crystal spatial light modulator. Applied Optics, 36 (1997), 1517–1520.

[4] Michaël A. F. Roelens, Jeremy A. Bolger, David Williams, Benjamin J. Eggleton, Multi-wavelength synchronous pulse burst generation with a wavelength selective switch, Opt. Express 2008; 16(14): 10152-10157.

[5] M. Gruneisen, et. al, Holographic correction in mid-IR using OA LC SLM elements, High–ResolutionWavefront Control: Methods, Devices, and Applications II, Proc. SPIE 2000; Vol. 4124.

[6] T. Martinez, D. V. Wick, S.R. Restaino, Foveated wide field-of-view imaging system using a liquid crystal spatial light modulator, Opt. Express 2001; 8: 555-560.

[7] D. J. Cho, S.T. Thurman, J.T. Donner, G.M. Morris, Characterization of a 128x128 liquid-crystal spatial light modulator for wave-front generation, Opt. Lett. 1998; 23(12): 969-971.

[8] Bougrenet de la Tocnaye J. L. and Dupont L., Complex amplitude modulation by use of liquid-crystal spatial light modulators, Appl. Opt. 1997, 36 1730–41.

[9] Duran V., Lancis J., Tajahuerce E. and Jaroszewicz Z., Equivalent retarder–rotator approach to on-state twisted-nematic liquid crystal displays, J. Appl. Phys., 2006 99 113101.

[10] S. Mias, N. Collings, R. Chittick, S. Coomber, M.Stanley, T. Wilkinson, W.A. Crossland, Spatial Sampling in Pixelated Metal Mirrored Ferroelectric Liquid Crystal Optically Addressed Spatial Light Modulator devices, Optical Engineering, Vol.42, No.7, p.2075-2081, July 2003.

[11] www2.ph.ed.ac.uk/~wjh/teaching/mo/slides/slms/slm.pdf.

[12] Wolfgang Osten, Christian Kohler and Jan Liesener, Evaluation and application of spatial light modulators for optical metrology, ÓPTICA PURA Y APLICADA, Vol. 38, No. 3, 2005.

[13] Holoeye Photonics AG and Holoeye Corporation. www.Holoeye.com.

[14] Fujitsu Semiconductor Ltd (2007) Wafer foundry service. FIND Vol.25 No.1.

[15] Grigory Lazarev, Andreas Hermerschmidt, Sven Krüger, and Stefan Osten, LCoS Spatial Light Modulators: Trends and Applications, Optical Imaging and Metrology: Advanced Technologies, First Edition, Wiley-VCH Verlag GmbH & Co. KGaA, 2012.

[16] J. P. Zonneveld, Using a Spatial Light Modulator to Efficiently Couple Light to Photonic Crystal Modes, UCSB, 2011.

[17] J. Leach, M. J. Padgett. Observation of chromatic effects near a white-light vortex. New Journal of Physics 5 (2003), 154.1–154.7

[18] J. L. Pezzaniti and R. A. Chipman, Phase-only modulation of a twisted nematic liquid-crystal TV by use of the eigenpolarization states, Opt. Lett. 18, 1567–1569, 1993.

[19] J. A. Davis, I. Moreno, and P. Tsai, Polarization eigenstates for twisted-nematic liquid-crystal displays, Appl. Opt. 37, 937–945, 1998.

[20] F. H. Yu and H. S. Kwok, Comparison of extended Jones matrices for twisted nematic liquid-crystal displays at oblique angles of incidence, J. Opt. Soc. Am. A 16, 2772–2780, 1999.

[21] A. Marquez, C. Iemmi, I. Moreno, J. A. Davis, J. Campos, and M. J. Yzuel, Quantitative predict of the modulation behavior of twisted nematic liquid crystal displays based on a simple physical model, Opt. Eng. 40, 2558–2564, 2001.

[22] I. Moreno, P. Velasquez, C. R. Fernandez-Pousa, M. M. Sanchez- Lopez, and F. Mateos, Jones matrix method for predicting and optimizing the optical modulation properties of a liquid-crystal display, J. Appl. Phys. 94, 3697–3702, 2003.

[23] C. Kohler, T. Haist and W. Osten, Model-free method for measuring the full Jones matrix of reflective liquid-crystal displays, Opt. Eng. 48(4), 044002, 2009.

[24] A. Michalkiewicz, M. Kujawinska, J. Kretzel, L. Salbut, X. Wang, and P. J. Bos, Phase manipulation and optoelectronic reconstruction of digital holograms by means of LCoS spatial light modulator, Proc. SPIE 5776, 144152, 2005.

[25] C. Kohler, X. Schwab, and W. Osten, Optimally tuned spatial light modulators for digital holography, Appl. Opt. 45, 960–967, 2006.

[26] M. Reicherter, S. Zwick, T. Haist, C. Kohler, H. Tiziani, and W. Osten, Fast digital hologram generation and adaptive force measurement in liquid-crystal-display-based holographic tweezers, Appl. Opt. 45, 888–896, 2006.

[27] C. Kohler, T. Haist, X. Schwab, and W. Osten, Hologram optimization for

SLM-based reconstruction with regard to polarization effects, Opt. Eng. 16, 14853–14861, 2008.

[28] C. Jones, A new calculus for the treatment of optical systems IV, J. Opt. Soc. Am. 31, 488, 1942.

[29] R. M. A. Azzam and N. M. Bashara, Ellipsometry and Polarized Light, North-Holland Publishing, Amsterdam, 1977.

[30] C. Brousseau, Fundamentals of Polarized Light, A Statistical Approach, Wiley, Hoboken, NJ, 1998.

[31] L. G. Neto, D. Roberge, and Y. Sheng, Programmable optical phasemostly holograms with coupled-mode modulation liquid-crystal television, Appl. Opt. 34, 1944–1950, 1995.

[32] K. Lu and B. E. A. Saleh, Theory and design of the liquid crystal TV as an optical spatial phase modulator, Opt. Eng. 29, 240–246, 1990.

[33] I. Moreno, J. A. Davis, K. G. D'Nelly, and D. B. Allison, Transmission and phase measurement for polarization eigenvectors in twisted nematic liquid crystal displays, Opt. Eng. 37, 3048–3052, 1998.

[34] Moreno, Fernández-Pousa, Franich and Davis, Polarization eigenvectors for reflective twisted nematic liquid crystal displays, Opt. Eng. 40(10) 2220–2226 (October 2001).

[35] A. Márquez, I. Moreno, C. Iemmi, A. Lizana, J. Campos, and M. J. Yzuel, Mueller-Stokes characterization and optimization of a liquid crystal on silicon display showing depolarization, Opt. Express, Vol. 16, No. 3: 1669-1685, 2008.

[36] J. E. Wolfe and R. A. Chipman, Polarimetric characterization of liquid-crystal-on-silicon panels, Appl.Opt. 45, 1688-1703 (2006).

[37] IEC 61947-1:2002. Electronic Projection. Measurement and documentation of

key performance criteria. Part 1: Fixed resolution projectors, IEC (International Electrotechnical Commission), Geneva, 2002.

[38] D. Goldstein, Polarized Light (Marcel Dekker, 2004).

[39] A. Márquez, J. Campos, M. J. Yzuel, I. Moreno, J. A. Davis, C. Iemmi, A. Moreno and A. Robert, Characterization of edge effects in twisted nematic liquid crystal displays, Opt. Eng. 39, 3301-3307 (2000).

[40] Q. Wang and S. He, A new effective model for the director distribution of a twisted nematic liquid crystal cell, J. Opt. A: Pure Appl. Opt. 7, 438-444 (2005).

[41] I. Moreno, P. Velásquez, C. R. Fernández-Pousa, M. M. Sánchez-López and F. Mateos, Jones matrix method for predicting and optimizing the optical modulation properties of a liquid-crystal display, J. Appl. Phys. 94, 3697-3702 (2003).

[42] V. Durán, J. Lancis, E. Tajahuerce, and Z. Jaroszewicz, Equivalent retarder-rotator approach to on-state twisted nematic liquid crystal displays, J. Appl. Phys. 99, 113101-113106 (2006).

[43] Guigay, On Fresnel diffraction by one-dimensional periodic objects, with application to structure determination of phase objects, Opt. Acta, 18; 677–82, 1971.

[44] Arrizon and Ojeda-Castañeda , Irradiance at Fresnel planes of a phase grating, J. Opt. Soc. Am. A, 9; 1801–6, 1992.

[45] Serrano-Heredia, Lu, Purwosumarto and Yu, Measurement of the phase modulation in liquid crystal television based on the fractional-Talbot effect, Opt. Eng. 35; 2680–4, 1996.

[46] Jaroszewicz, Kołodziejczyk, Kowalik and Restrepo, Determination of the step

height of the binary phase grating from its Fresnel images, Optik, 111; 207–10, 2000.

[47] Spence, and Qian, Irradiance at Fresnel planes of a phase grating, Phys. Rev. B, 45; 10271–80, 1992.

[48] Cloetens, Guigay, De Martino, Baruchel and Schlenker, Fractional Talbot imaging of phase gratings with hard x rays, Opt. Lett. 22; 1059–61, 1997.

[49] Riley Jr, Optical determination of low ultrasonic powers, J. Acoust. Soc. Am., 67; 1386–8, 1980.

[50] Martínez-León, Z. Jaroszewicz, A. Kołodziejczyk, V. Durán, E. Tajahuerce and J. Lancis, Phase calibration of spatial light modulators by means of Fresnel images, J. Opt. A: Pure Appl. Opt. 11 (2009) 125405.

[51] I. Moreno, A. Lizana, J. Campos, A. Márquez, C. Iemmi, and M. J. Yzuel, Combined Mueller and Jones matrix method for the evaluation of the complex modulation in a liquid-crystal-on-silicon display," Opt. Lett. 33(6), 627–629 (2008).

[52] A. Márquez, C. Iemmi, I. Moreno, J. A. Davis, J. Campos, and M. J. Yzuel, Quantitative prediction of the modulation behavior of twisted nematic liquid crystal displays based on a simple physical model, Opt. Eng. 40(11), 2558–2564 (2001).

[53] C. Soutar, Measurement of the complex transmittance of the Epson liquid crystal television, Opt. Eng. 33(4), 1061–1068 (1994).

[54] D. Engström, G. Milewski, J. Bengtsson, and S. Galt, Diffraction-based determination of the phase modulation for general spatial light modulators, Appl. Opt. 45(28), 7195–7204 (2006).

[55] L. G. Neto, D. Roberge, and Y. Sheng, Programmable optical phase-mostly

holograms with coupled-mode modulation liquid-crystal television, Appl. Opt. 34(11), 1944–1950 (1995).

[56] Flávio P. Ferreira and Michael S. Belsley, Direct calibration of a spatial light modulator by lateral shearing interferometry, Opt. Express, 18, No. 8, 7899-7904, 2010.

[57] Grother P and Casasent, Optical path difference measurement techniques for SLMs Opt. Commun. 2001, 189 31–8.

[58] Mok F, Diep J H, Liu H-K and Psaltis, Real-time computer-generated hologram by means of liquid-crystal television spatial light modulator Opt. Lett. 1986, 11 748–50.

[59] Zhang H., Zhang J. and Wu L., Evaluation of phase-only liquid crystal spatial light modulator for phase modulation performance using a Twyman–Green interferometer, Meas. Sci. Technol. 2007, 18 1724–8.

[60] A. Lizana, I. Moreno, A. Ruiz Márquez, C. Iemmi, J. Campos and M. J. Yzuel, Characterization and Analysis of LCoS displays: Application to Diffractive Optics, Proc. of SPIE, 2009, Vol. 7442 74420Y-3, CCC code: 0277-786X/09/$18 · doi: 10.1117/12.829221.

[61] M. Born and E. Wolf, Principles of Optics, Pergamon, Oxford, 1970.

[62] Oded Kafri and Ilana Glatt, The physics of moiré metrology, John Wiley & Sons, 1990.

[63] Daniel Malacara, Optical Shop Testing, Wiley, 3ed., 2007.

[64] K. Patorski, Handbook of the moiré fringe technique, Elsevier, 1993.

[65] Asundi A, Yung KH. Phase-shifting and logical moiré. J. Opt. Soc. Am. A 1991;8(10):1591–600.

[66] Yokozeki, S., and T. Suzuki, Modified double-beam interferometer using the moiré method, Appl. Opt.11, 446-448,1972.

[67] Yokozeki, S., and T. Suzuki, Modified double-beam interferometer using the moiré method, Part 2, Appl. Opt.11, 2715-2717, 1972.

[68] Yokozeki, S., and T. Suzuki, Modified double-beam interferometer using the moiré method, Part 3, Appl. Opt.12, 412-414, 1973.

[69] K. Jambunathan, L. S. Wang, B. N. Dobbins, and S. P. He, Semi- automatic phase shifting calibration using digital speckle pattern interferometry, Opt. Laser Tech. 27, 145–151, 1995.

[70] Ochoa and Huntley, Convenient method for calibrating nonlinear phase modulators, Opt. Eng. 37(9) 2501–2505 (September 1998).

[71] Soutar C, Lu K. Determination of the physical properties of an arbitrary twisted-nematic liquid crystal cell. Opt. Eng. 1994;33(8):2704–12.

[72] Yamaguchi M, Márquez A, Davis J.A, Franich D.J., Interferometric phase measurements for polarization eigenvectors in twisted nematic liquid crystal spatial light modulators. Opt Commun 2000;181:1–6.

[73] A. Lizana, I. Moreno, A. Ruiz Márquez, C. Iemmi d , J. Campos and M.J.Yzuel, Characterization and Analysis of LCoS displays: Application to Diffractive Optics, Optics and Photonics for Information Processing III, Proc. of SPIE Vol. 7442, 74420Y, 2009

[74] Lizana A, Moreno I, Márquez A, Iemmi C, Fernández E, Campos J, et al. Time fluctuations of the phase modulation in a liquid crystal on silicon display: characterization and effects in diffractive optics. Opt Express 2008;16: 16711–22.

[75] Benzie P, Watson J, Surman P, Rakkolainen I, Hopf K, Urey H, et al. A survey of 3DTV displays: techniques and technologies. IEEE Tans Circuits Syst Video Technol 2007;17:1647–58.

[76] C. Y. Calderón-Hermosillo, J. García-Márquez, N. Alcala-Ochoa, V. López, A.

Aguilar, E. Noé-Arias, Yasser Alayli, Flicker in a twisted nematic spatial light modulator, Optics and Lasers in Engineering, 51 (2013) 741–748.

[77] Lizana A, Márquez A, Moreno I, Iemmi C, Campos J, Yzuel MJ. Wavelength dependence of polarimetric and phase-shift characterization of a liquid crystal on silicon display, J Eur Opt Soc—Rapid Publ 2008;3(08012): 1–6.

[78] Lizana A, Moreno I, Iemmi C, Márquez A, Campos J, Yzuel MJ. Time-resolved Mueller matrix analysis of a liquid crystal on silicon display, Appl Opt 2008;47:4267–74.

[79] Verma RS, Swami MK, Manhas SS, Gupta PK. Mueller matrix-based optimization of reflective type twisted nematic liquid crystal SLM at oblique incidences, Opt Commun 2010;283:2580–7.

[80] Durán V, Clemente P, Martínez-León L, Climent V, Lancis J. Poincaré-sphere representation of phase-mostly twisted nematic liquid crystal spatial light modulators, J Opt A: Pure Appl Opt 2009;11(085403):1–8.

[81] Lizana A, Márquez A, Lobato L, Rodange Y, Moreno I, Iemmi C, et al. The minimum Euclidean distance principle applied to improve the modulation diffraction efficiency in digitally controlled spatial light modulators, Opt. Express 2010;18:10581–93.

[82] García-Márquez Jorge, López Victor, González-Vega Arturo, Noé Enrique, Flicker minimization in an LCoS spatial light modulator. Opt. Express 2012;20:8431–41.

[83] Salas-Alcántara K. M., Torres-Gómez I., Polarimetric Mueller – Stokes analysis of photonic crystal fibers with mechanically-induced long-period gratings. Opt. Eng. 2012;51(8):085005, http://dx.doi.org/10.1117/1.OE.51.8.085005.

[84] C.Y. Calderón-Hermosillo, N. Alcala-Ochoa, E. Noé-Arias, J. García-Márquez,

Inspection of complex amplitudes of spatial light modulators using moiré techniques, Optics and Lasers in Engineering, vol. 51 (2013) 610–615.